The Pennsylvania State University

The Graduate School

Eberly College of Science

METAL ATOM-MOLECULE INTERACTIONS IN SELF-ASSEMBLED MONOLAYERS

A Thesis in

Chemistry

by

Timothy B. Tighe

Submitted in Partial Fulfillment

of the Requirements

for the Degree of

Doctor of Philosophy

December 2003

The thesis of Timothy B. Tighe was reviewed and approved* by the following

David L. Allara
Professor of Materials Science and Chemistry
Thesis Advisor
Chair of Committee

Nicholas Winograd
Evan Pugh Professor of Chemistry

Thomas E. Mallouk
Dupont Professor of Materials Chemistry

Carlo G. Pantano
Distinguished Professor of Materials Science and Engineering

Andrew G. Ewing
Professor of Chemistry
Head of the Department of Chemistry

*Signatures are on file in the Graduate School

Chapter 1

Introduction: Metallization of Organic Films

1.1 Overview

Understanding the atomic and molecular level interactions of metal atoms with organic surfaces is becoming increasingly important as the number of applications involving metal-organic interfaces grows. There has been a longstanding general interest in the metallization of polymers. Recently, there has been increasing interest in the emerging fields of polymer and molecular electronic devices in which the issue of optimizing top-metal contacts is of critical importance. Given the complexity of these structures in terms of chemical interactions and metal film morphology, and given the wide range of choices in metals, organic materials and deposition conditions, the rational design of metal/organic structures requires a broad, fundamental understanding of the mechanistic and thermodynamic aspects of metal atom-molecule interactions. The spectrum of interactions can be quite varied, ranging from weak adsorption, which could lead to clustering with poor adhesion and/or electrical contact and diffusion into the bulk, to strong chemical reaction with severe destruction of chemical integrity. Recent efforts to explore fundamental interactions have focused on the use of self-assembled monolayers (SAMs) because of their highly organized surface structures with uniform density of organic groups that allow quantitative characterization of the metal-molecule interactions. This approach is directly relevant to molecular electronic devices whose core structures depend upon SAMs, typically with vacuum deposited metal contacts. On a more fundamental level, these types of experiments add a new strategy to the study of organometallic chemistry by providing quantitative probes of metal atom interactions with organic functional groups in well-defined geometries under highly controlled conditions.

This introductory chapter will be broken up into two parts. The first part will discuss the field of deposited metal/polymer interfaces, with and emphasis on research preformed in the areas of polymer light emitting diodes, photovoltaic devices, and microelectronics. The second part will cover the metallization of self-assembled monolayers as models for polymer systems and the metallization of self-assembled monolayer-based electronics.

1.2 Metal/Polymer Interfaces

The study of metal/polymer interfaces began in earnest in the late 1970's and early 1980's [1-10]. Since that time, metallized polymers have found their way into many common items used today, such as shiny reflecting parts for cars and jewelry, compact disks, computer cases, and even food packaging [11-18]. No area of metallized polymers has generated as much interest or research as the area of semi-conducting and conducting polymers for use in microelectronics and polymer light emitting diodes.

Understanding the chemical and physical nature of the metal/polymer interface is of paramount importance when considering materials for devices. The type of device dictates the desired interaction. For instance, a simple polymer light emitting diode consists of three materials; a thin polymer layer sandwiched between a pair of electrodes. The negative electrode, usually a thermally evaporated low work function metal, injects electrons into the polymer film while the positive electrode, a high work function optically transparent material, injects holes. The electron and hole polarons migrate through the film because of the electric field. If electron and hole polarons meet they can combine, emitting light that is free to leave the device through the optically transparent positive electrode. The positive electrode has a high work function, so it can pull

electrons away from the polymer and is optically transparent in order for generated light to escape the device. Indium tin oxide is commonly used as the positive electrode. The negative electrode should ideally be a metal with a low work function that matches the electron affinity of the polymer [26,30]. In this application the chemical nature of the deposited metal contact is a key aspect of ensuring proper device performance. Strong chemical interaction with polymeric constituents or diffusion into the polymer could drastically alter the properties of the polymer and ruin the device. Clustered metal growth could result in a dielectric layer at the interface, which would have a much higher work function than desired for the device. This could result in higher driving voltages, higher power consumption, and shorter life times, if not complete device failure [30]. While this is just one simple example of how important the metal/polymer interface is to device efficiency, one can imagine that the more complex the device, the greater the precision necessary in making precise metallic contacts.

The study of metal on polymers proceeded in roughly two paths. The first path has involved the performance of more fundamental studies in order to gain a better understanding of the chemistry at the metal/polymer interface or interphase. Work in this area has predominantly involved the metals Au, Ag, Cu, Pd, and Cr, although other metals such as Fe, Ni, K, and Ti have been included at times [20,23,25,28,31-52]. The second path has been much more device oriented. Metals and polymers are chosen because of their intrinsic properties, and combinations are more of a “hit or miss” style of experimentation. It has been the field of polymer light emitting diodes that has driven this research, so it only stands to reason that it is dominated by studies involving low work function metals such as Al, Ca, Na, K, Mg, alloys of Ag:Mg, and diffusion barriers

of Cr and Ti [19,21,22,24,27,29,31,53-75]. When surveyed, the literature reveals a strong correlation between metal polymer chemical interaction, metal diffusivity, and the metal film nucleation and growth process. Simply put, the weakly interacting metals Cu, Ag, and Au were found to diffuse deeply into the bulk of the polymers studied and form clusters while the highly reactive metals Cr and Ti interact strongly with the polymers and form relatively sharp interfaces. The behavior of Al and Ni was found to fall somewhere between these two groups, while those of the alkali metals Na, K, Rb, and Cs proved to be able to reduce the conducting polymers and diffuse throughout as highly mobile cations [23].

Nucleation and subsequent growth of metal clusters can be influenced by a number of factors. A few of these include substrate temperature, deposition rate, number of trapping sites, energy of the deposited metal, etc. To form an interface with the desired chemical, physical, or electronic properties, a detailed understanding of the competition between these different processes during film growth, under well defined conditions, is critical [28]. To complicate matters further, one must first have an idea of the chemical nature of the interface on which the metals are being deposited. This is a specific area that has made the study of metal-polymer interfaces difficult. Polymer conformation and dynamics will dictate the orientation and mobility of polymer functional groups, making the interface highly complex. It was as a means of solving the issue of a poorly characterized interface that the use of self-assembled monolayers (SAMs) was introduced.

1.3 Metal/SAM Interfaces

SAMs are ordered molecular assemblies formed by the adsorption of an active surfactant on a solid surface. SAMs have been constructed with a variety of chemisorbing head group/substrate pairs along with many different terminal functional groups [72-74]. At the start of the 1990's Czanderna and co workers at the National Renewable Energy Lab discovered the benefits to using SAMs as model organic interfaces. It was noted that the ability to assemble SAMs with highly controlled quantities, types, and orientations of organic functional groups exposed at the interface could allow for unprecedented quantitative studies in the area of organometallic interactions [75-95]. The combined works of Czanderna, Jung, Herdt, King, Tarlov, Konstadinidis et. al., have been summarized in numerous review articles [31,87,91,92]. In this pioneering work, the usefulness alkanethiols self-assembled on gold as model interfaces was investigated. It was found that the nature of the deposited metal film depended on the strength of the metal/organic functional group interaction. Three very important points came out of this initial research. Firstly, the extent of interaction between the metal and the organic functional group played an important role on the morphology of the metal film growth. Very weak interactions led to metal penetration, weak to medium physical/chemical interactions led to larger sized cluster growth on the surface, and strong interactions led to smaller cluster sized growth (though no smooth, uniform metallic layers were reported). Secondly, the chain length of the alkyl chain had an effect on penetrating systems, the longer the chain, the slower the penetration. And thirdly, the substrate temperature had an effect on penetration rates as well. It was found that lower temperatures reduced the rate of penetration. Penetration could be stopped below a

certain temperature, however, upon warming, the metals were then found to penetrate. They were also able to put a reactivity matrix together for the metal systems studied. In summary it was found that: the metal's reactivity were ranked Ti>Cr>Al,Ni>Cu>Ag and the reactivity's of the organic functional groups were ranked $COOCH_3$, CN>COOH>OH>CH_3.

Since these initial studies with metals on SAMs, there have been a number of other studies done. Single layers of molecules have been patterned on a surface by microcontact printing. These patterned surfaces served as activation templates for metal chemical vapor deposition and allowed fabrication of sharp metal line patterns of Cu, Pt, and Pd [96-98]. Ag, Cu, and Ca have also been deposited onto thiol and phosphate modified gold electrodes by means of electrochemical deposition, chemical vapor deposition, and underpotential deposition [99-116]. Ohgi et. al. and others have done numerous studies on the growth of Au, and Ag nanoclusters on thiol and dithiol monolayers [117-122,130]. The dithiol is used in attempts to prevent penetration of the metal atoms to the Au/S interface by providing metal cluster nucleation sites. Initial studies using silane monolayers on SiO_2 as diffusion barriers for copper deposition and nucleation sites for Au nanoclusters have also been reported [124-128]. Some previously studied systems have been reinvestigated using other analytical techniques or novel deposition techniques as was the case for Cu on dodecanethiol and octadecanethiol [129] and metal-organic chemical vapor deposition of $Al_xO_yH_z$ on hydroxyl-terminated monolayers.

Recent collaborations between the Allara and Winograd groups, along with contributions from other research groups at Pennsylvania State University and scientists

in industry, have studied the interaction of Al atoms with a variety of terminal groups including -CO_2CH_3, -COOH, -OH, -OCH_3, and -CH_3 [132-135]. The deposited Al was found to have: a) reacted with the terminal group to form organoaluminum complexes (-CO_2CH_3, -COOH and -OH); b) penetrated to the Au/S interface (-CH_3); and c) simultaneously penetrated to the Au/S interface and interacted with terminal group (-OCH_3). This was the basis for the research conducted in chapters 2 through 5.

Molecules have many attractive properties for use in electronic devices including their cost, relative stability, synthetic flexibility and small size [136,137]. A variety of molecular analogues of silicon-based electronic devices have been demonstrated, including switches [138], rectifying diodes [139-142], negative differential resistance devices [143,144] for random access memory cells [145] and transistors [146]. However, there are still many challenges to be overcome in device fabrication; at present, significant device-to-device variation has been observed [143,144]. Many devices are fabricated by self-assembling the device molecules on a bottom contact, typically gold, (typical diameter < (30-50) nm) and then forming top contact by depositing metal on this structure using physical vapor deposition (thermal evaporation) [144]. However it can be difficult to make stable, noninvasive top metallic contacts. Recent literature has started to address the interactions of metals with organic functional groups contained in these devices [147-151], however, much more information is needed. This is the driving force behind the research in chapter 6 and future planned research.

In conclusion this collection of studies is designed to provide a fundamental understanding of the pathways of chemical reactions and interactions of SAMs with deposited metal atoms. From this data and future studies, we shall be able to better design

and control the formation of many different metallized organic structures, which is useful in applications, such as molecular or organic electronics, where control of the metal-molecule interface is crucial.

REFERENCES

1. Fabish, T. J.; Saltsburg, H. M.; Hair, M. L. Charge Transfer in Metal/Atactic Polystyrene Contacts. *J. Appl. Phys.* **1976,** *47,* 930-939.

2. Mittal, K. L. Adhesion aspects of metallization of organic polymer surfaces. *J. Vac. Sci. Technol.* **1976,** *13* , 19-25.

3. Burkstrand, J. M. Formation of metal-oxygen-polymer complexes on polystyrene with nickel and chromium. *J. Vac. Sci. Technol.* **1979,** *16* , 1072-1074.

4. Burkstrand, J. M. Core-Level spectra of chromium and nickel atoms on polystyrene. *J. Appl. Phys.* **1979,** *50,* 1152-1153.

5. Burkstrand, J. M. Copper-polyvinyl alcohol interface:A study with XPS. *J. Vac. Sci. Technol.* **1979,** *16,* 363-365.

6. Burkstrand, J. M. Substrate effects on the electronic structure of metal overlayers. *Phys. Rev. B* **1979,** *20* , 4853-4858.

7. Burkstrand, J. M. Metal-polymer interfaces: Adhesion and x-ray photoemission studies. *J. Appl. Phys.* **1981,** *52* , 4795-4800.

8. Barthell, B. L.; Duchane, D. V. Vacuum deposition of High quality metal films on porous substrates. *J. Vac. Sci. Technol.* **1982,** *20* , 1341-1344.

9. Burkstrand, J. M. Hot atom interactions with polymer surfaces. *J. Vac. Sci. Technol.* **1982,** *21* , 70-73.

10. Burkstrand, J. M. Summary Abstract: Chemical interactions at polymer-metal interfaces and the correlation with adhesion. *J. Vac. Sci. Technol.* **1982,** *20,* 440-441.

11. Lee, L. H.; (Ed.) Fundamentals of Adhesion. Plenum Press: New York, New York , 1990.

12. Mittal, K. L.; (Ed.) Metallized Plastics 2: Fundamental and Applied Aspects. Plenum Press : New York, New York , 1992.

13. Mittal, K. L.; (Ed.) Metallized Plastics 3: Fundamental and Applied Aspects. Plenum Press: New York, New York, 1992.

14. Mittal, K. L.; Lee, K. W.; (Eds.) Polymer Surfaces and Interfaces: Characterization, Modification, and Application. VSP: Utretch, The Netherlands, 1997.

15. Mittal, K. L.; (Ed.) Metallized Plastics: Fundamentals and Applications. Marcel Dekker: New York, New York , 1998.

16. Mittal, K. L.; (Ed.) Metallized Plastics 5&6: Fundamental and Applied Aspects. VSP: Utretch, The Netherlands , 1998.

17. Mittal, K. L.; (Ed.) Metallized Plastics 7: Fundamental and Applied Aspects. VSP: Utretch, The Netherlands, 2001.

18. Susko, J. R.; Mittal, K. L.; (Eds.) Metallized Plastics: Fundamental and Applied Aspects. Plenum Press: New York, New York, 1990.

19. Salaneck, W. R.; Bredas, J. L. The metal-on-polymer interface in polymer light emitting diodes. *Adv. Mater.* **1996,** *8,* 48-&.

20. Strunskus, T.; Grunze, M.; Kochendoerfer, G.; Woll, C. Identification of physical and chemical interaction mechanisms for the metals gold, silver, copper, palladium, chromium, and potassium with polyimide surfaces. *Langmuir* **1996,** *12,* 2712-2725.

21. Salaneck, W. R.; Logdlund, M.; Birgersson, J.; Barta, P.; Lazzaroni, R.; Bredas, J. L. Electronic and chemical structure of conjugated polymer surfaces and interfaces: Implications for polymer-based electronic devices. *Synthetic. Met.* **1997,** *85,* 1219-1220.

22. Salaneck, W. R.; Bredas, J. L. Conjugated polymer surfaces and interfaces for light-emitting devices. *Mrs Bulletin* **1997,** *22,* 46-51.

23. Faupel, F.; Willecke, R.; Thran, A. Diffusion of metals in polymers. *Mat. Sci. Eng. R* **1998,** *22,* 1-55.

24. Kugler, T.; Logdlund, M.; Salaneck, W. R. Polymer surfaces and interfaces in light-emitting devices. *Ieee Journal of Selected Topics in Quantum Electronics* **1998,** *4,* 14-23.

25. Strunskus, T.; Kiene, M.; Willecke, R.; Thran, A.; von Bechtolsheim, C.; Faupel, F. Chemistry, diffusion and cluster formation at metal-polymer interfaces. *Mater. Corros.* **1998,** *49,* 180-188.

26. Friend, R.; Burroughes, J.; Shimoda, T. Polymer diodes. *Phys. World* **1999,** *12,* 35-40.

27. Kugler, T.; Logdlund, M.; Salaneck, W. R. Photoelectron spectroscopy and quantum chemical modeling applied to polymer surfaces and interfaces in light-emitting devices. *Acc. Chem. Res.* **1999,** *32*, 225-234.

28. Strunskus, T.; Zaporojtchenko, V.; Behnke, K.; von Bechtolsheim, C.; Faupel, F. Tailoring the morphology of metal/polymer interfaces. *Adv. Eng. Mat.* **2000,** *2*, 489-492.

29. Salaneck, W. R.; Logdlund, M.; Fahlman, M.; Greczynski, G.; Kugler, T. The electronic structure of polymer-metal interfaces studied by ultraviolet photoelectron spectroscopy. *Mat. Sci. Eng. R* **2001,** *34*, 121-146.

30. Fahlman, W.; Salaneck, W. R. Surfaces and interfaces in polymer-based electronics. *Surf. Sci.* **2002,** *500*, 904-922.

31. Opila, R. L.; Eng, J. Thin films and interfaces in microelectronics: composition and chemistry as function of depth. *Prog. Surf. Sci.* **2002,** *69*, 125-163.

32. Tromp, R. M.; LeGoues, F. K.; Ho, P. S. Interdiffusion at the polyimide-Cu interface. *J. Vac. Sci. Technol. A* **1985,** *3* , 782-785.

33. White, R. C.; Haight, R.; Silverman, B. D.; Ho, P. S. Cr-Polyimide and Cu-Polyimide Interface - Chemistry and Structure. *Appl. Phys. Lett.* **1987,** *51*, 481-483.

34. Faupel, F.; Gupta, D.; Silverman, B. D.; Ho, P. S. Direct Measurements of Cu Diffusion Into A Polyimide Below the Glass-Transition Temperature. *Appl. Phys. Lett.* **1989,** *55*, 357-359.

35. Faupel, F.; Yang, C. H.; Chen, S. T.; Ho, P. S. Adhesion and Deformation of Metal Polyimide Layered Structures. *J. Appl. Phys.* **1989,** *65*, 1911-1917.

36. Strunskus, T.; Hahn, C.; Frankel, D.; Grunze, M. Interaction of Evaporated Copper with Vapor-Deposited Thin Polyimide Films. *J. Vac. Sci. Technol. A* **1991,** *9*, 1272-1277.

37. Willecke, R.; Faupel, F. Diffusion of gold and silver in bisphenol a polycarbonate. *Macromolecules* **1997,** *30*, 567-573.

38. Willecke, R.; Faupel, F. Diffusion of gold and silver in bisphenol trimethylcyclohexanen polycarbonate. *Journal of Polymer Science Part B-Polymer Physics* **1997,** *35*, 1043-1048.

39. Faupel, F.; Willecke, R.; Thran, A.; Kiene, M.; vonBechtolsheim, C.; Strunskus, T. Metal diffusion in polymers. *Defect and Diffusion Forum* **1997,** *143*, 887-902.

40. Southward, R. E.; Thompson, D. W. Inverse CVD: A novel synthetic approach to metallized polymeric films. *Adv. Mater.* **1999,** *11,* 1043-1047.

41. von Bechtolsheim, C.; Zaporojtchenko, V.; Faupel, F. Interface structure and formation between gold and trimethylcyclohexane polycarbonate. *J. Mater. Res.* **1999,** *14,* 3538-3543.

42. von Bechtolsheim, C.; Zaporojtchenko, V.; Faupel, F. Influence of thermal treatment on the morphology and adhesion of gold films on trimethylcyclohexane-polycarbonate. *Appl. Surf. Sci.* **1999,** *151,* 119-128.

43. Strunskus, T.; Zaporojtchenko, V.; Behnke, K.; von Bechtolsheim, C.; Faupel, F. Tailoring the morphology of metal/polymer interfaces. *Adv. Eng. Mat.* **2000,** *2,* 489-492.

44. Zaporojtchenko, V.; Behnke, K.; Thran, A.; Strunskus, T.; Faupel, F. Condensation coefficients and initial stages of growth for noble metals deposited onto chemically different polymer surfaces. *Appl. Surf. Sci.* **1999,** *145,* 355-359.

45. Zaporojtchenko, V.; Behnke, K.; Strunskus, T.; Faupel, F. Determination of condensation coefficients of metals on polymer surfaces. *Surf. Sci.* **2000,** *454,* 412-416.

46. Zaporojtchenko, V.; Strunskus, T.; Behnke, K.; von Bechtolsheim, C.; Thran, A.; Faupel, F. Formation of metal-polymer interfaces by metal evaporation: influence of deposition parameters and defects. *Microelectron. Eng.* **2000,** *50,* 465-471.

47. Zaporojtchenko, V.; Strunskus, T.; Behnke, K.; von Bechtolsheim, C.; Kiene, M.; Faupel, F. Metal/polymer interfaces with designed morphologies. *J. Ahes. Sci. Techno.* **2000,** *14,* 467-490.

48. Zaporojtchenko, V.; Behnke, K.; Strunskus, T.; Faupel, F. Condensation coefficients of noble metals on polymers: a novel method of determination by x-ray photoelectron spectroscopy. *Surf. Interface Anal.* **2000,** *30,* 439-443.

49. Zaporojtchenko, V.; Strunskus, T.; Erichsen, J.; Faupel, F. Embedding of noble metal nanoclusters into polymers as a potential probe of the surface glass transition. *Macromolecules* **2001,** *34,* 1125-1127.

50. Thran, A.; Strunskus, T.; Zaporojtchenko, V.; Faupel, F. Evidence of noble metal diffusion in polymers at room temperature and its retardation by a chromium barrier. *Appl. Phys. Lett.* **2002,** *81,* 244-246.

51. Carlo, S. R.; Perry, C.; Torres, J.; Fairbrother, D. H. Metallization of poly(vinylchloride) by Fe, Ni, Cu, Ag, and Au. *J. Vac. Sci. Technol. A* **2002,** *20,* 350-355.

52. Zaporojtchenko, V.; Zekonyte, J.; Biswas, A.; Faupel, F. Controlled growth of nano-size metal clusters on polymers by using VPD method. *Surf. Sci.* **2003,** *532,* 300-305.

53. Dannetun, P.; Boman, M.; Stafstrom, S.; Salaneck, W. R.; Lazzaroni, R.; Fredriksson, C.; Bredas, J. L.; Zamboni, R.; Taliani, C. The Chemical and Electronic-Structure of the Interface Between Aluminum and Polythiophene Semiconductors. *J. Chem. Phys.* **1993,** *99,* 664-672.

54. Dannetun, P.; Logdlund, M.; Fahlman, M.; Boman, M.; Stafstrom, S.; Salaneck, W. R.; Lazzaroni, R.; Fredriksson, C.; Bredas, J. L.; Graham, S.; Friend, R. H.; Holmes, A. B.; Zamboni, R.; Taliani, C. The Chemical and Electronic-Structure of the Interface Between Aluminum and Conjugated Polymers Or Molecules. *Synthetic. Met.* **1993,** *55,* 212-217.

55. Dannetun, P.; Logdlund, M.; Fredriksson, C.; Lazzaroni, R.; Fauquet, C.; Stafstrom, S.; Spangler, C. W.; Bredas, J. L.; Salaneck, W. R. Reactions of Low Work Function Metals Na, Al, and Ca on Alpha,Omega-Diphenyltetradecaheptaene - Implications for Metal/Polymer Interfaces. *J. Chem. Phys.* **1994,** *100,* 6765-6771.

56. Dannetun, P.; Fahlman, M.; Fauquet, C.; Kaerijama, K.; Sonoda, Y.; Lazzaroni, R.; Bredas, J. L.; Salaneck, W. R. Interface Formation Between Poly(2,5-Diheptyl-P-Phenylenevinylene) and Calcium - Implications for Light-Emitting-Diodes. *Synthetic. Met.* **1994,** *67,* 133-136.

57. Dekoven, B. M.; Hagans, P. L. Xps Studies of Metal Polymer Interfaces - Thin-Films of Al on Polyacrylic-Acid and Polyethylene. *Appl. Surf. Sci.* **1986,** *27,* 199-213.

58. Fredriksson, C.; Stafstrom, S. Metal/Conjugated Polymer Interfaces - Sodium, Magnesium, Aluminum, and Calcium on Transpolyacetylene. *J. Chem. Phys.* **1994,** *101,* 9137-9142.

59. Fung, M. K.; Lai, S. L.; Bao, S. N.; Lee, C. S.; Lee, S. T.; Wu, W. W.; Inbasekaran, M.; O'Brien, J. J. Interface between poly (9,9-dioctylfluorene) and alkali metals: cesium, potassium, sodium, and lithium. *J. Vac. Sci. Technol. A* **2002,** *20,* 911-918.

60. Gador, D.; Buchberger, C.; Soukopp, A.; Sokolowski, E.; Fink, R.; Umbach, E. Interaction of magnesium with oriented diphenyl-carbonate films. *J. Electron Spectrosc. Relat. Phenom.* **1999,** *103,* 529-537.

61. Kono, M.; Wong, P. C.; Li, Y. S.; Mitchell, K. A. R. X-ray photoelectron spectroscopy studies of

the stability of Al/Mg/PET interfaces. *Surf. Rev. Lett.* **2000,** *7*, 227-233.

62. Konstadinidis, K.; Papadimitrakopoulos, F.; Galvin, M.; Opila, R. L. In-Situ X-Ray Photoelectron-Spectroscopy Study of Aluminum/Poly (P-Phenylenevinylene) Interfaces. *J. Appl. Phys.* **1995,** *77*, 5642-5646.

63. Lazzaroni, R.; Bredas, J. L.; Dannetun, P.; Logdlund, M.; Uvdal, K.; Salaneck, W. R. Electronic-Structure of the Aluminum Polythiophene Interface - A Joint Experimental and Theoretical-Study. *Synthetic. Met.* **1991,** *43*, 3323-3328.

64. Lazzaroni, R.; Bredas, J. L.; Dannetun, P.; Fredriksson, C.; Stafstrom, S.; Salaneck, W. R. The Chemical and Electronic-Structure of the Interface Between Aluminum and Conjugated Polymers. *Electrochim. Acta* **1994,** *39*, 235-244.

65. Lazzaroni, R.; Logdlund, M.; Calderone, A.; Bredas, J. L.; Dannetun, P.; Fauquet, C.; Fredriksson, C.; Stafstrom, S.; Salaneck, W. R. Chemical and Electronic Aspects of Metal Conjugated Polymer Interfaces - Implications for Electronic Devices. *Synthetic. Met.* **1995,** *71*, 2159-2162.

66. Lim, V. W. L.; Kang, E. T.; Neoh, K. G.; Huang, W. In situ x-ray photoelectron spectroscopy study of evaporated magnesium on chemically synthesized polypyrrole films. *J. Vac. Sci. Technol. A* **2001,** *19*, 2680-2688.

67. Ma, Z. H.; Lim, S. L.; Tan, K. L.; Li, S.; Kang, E. T. In situ X-ray photoelectron spectroscopy studies of interactions of evaporated metals with electroactive polyaniline films. *J. Mater. Sci. - Mater. El.* **2000,** *11*, 311-317.

68. Ma, Z. H.; Lim, S. L.; Tan, K. L.; Li, S.; Kang, E. T. In situ X-ray photoelectron spectroscopy study of the interactions of evaporated magnesium with polyaniline films. *Surf. Sci.* **2000,** *454*, 995-999.

69. Murdey, R.; Stuckless, J. T. Calorimetry of polymer metallization: Copper, calcium, and chromium on PMDA-ODA polyimide. *J. Am. Chem. Soc.* **2003,** *125*, 3995-3998.

70. Nguyen, T. P.; Ip, J.; Jolinat, P.; Destruel, P. XPS and sputtering study of the Alq(3)/electrode interfaces in organic light emitting diodes. *Appl. Surf. Sci.* **2001,** *172*, 75-83.

71. Pireaux, J. J. Is There An Interaction at the Aromatic Site(S) in A Metal-Polymer Interface - An Xps and Hreels Review. *Synthetic. Met.* **1994,** *67*, 39-46.

72. Allara, D. L.; Nuzzo, R. G. *Langmuir* 1985, *1*, 45-52.

73. Dubois, L. H.; Nuzzo, R. G. *Ann. Rev. Phys. Chem.* **1992**, *43*, 437.

74. Scheiber, F. *Prog. Surf. Sci.* **2000**, *65*, 151-256.

75. Czanderna, A. W.; King, D. E.; Spaulding, D. Metal Overlayers on Organic Functional-Groups of Self-Organized Molecular Assemblies .1. X-Ray Photoelectron-Spectroscopy of Interactions of Cu/Cooh on 11-Mercaptoundecanoic Acid. *J. Vac. Sci. Technol. A* **1991,** *9,* 2607-2613.

76. Tarlov, M. J. Silver Metalization of Octadecanethiol Monolayers Self-Assembled on Gold. *Langmuir* **1992,** *8,* 80-89.

77. Herdt, G. C.; Czanderna, A. W. Penetration of Vacuum-Deposited Silver Into Octadecanethiol Self-Assembled Monolayers Studied with Iss. *Surf. Sci.* **1993,** *297,* L109-L112.

78. Jung, D. R.; King, D. E.; Czanderna, A. W. Xps of Organized Molecular Assembly Copper Interfaces - HS(CH2)11OH/Cu. *Appl. Surf. Sci.* **1993,** *70-1,* 127-132.

79. Jung, D. R.; King, D. E.; Czanderna, A. W. Metal Overlayers on Organic Functional-Groups of Self-Organized Molecular Assemblies .2. X-Ray Photoelectron-Spectroscopy of Interactions of Cu/Cn on 12-Mercaptododecanenitrile. *J. Vac. Sci. Technol. A* **1993,** *11,* 2382-2386.

80. King, D. E.; Czanderna, A. W.; Spaulding, D. X-Ray Photoelectron-Spectroscopy Analysis of the Copper Arachidic Acid Organized Molecular Assembly Interface - Charging Phenomena. *J. Vac. Sci. Technol. A* **1993,** *11,* 180-182.

81. Herdt, G. C.; Czanderna, A. W. Metal Overlayers on Self-Organized Molecular Assemblies .4. Ion-Scattering Spectroscopy of the Ag/Ch3 Interface. *J. Vac. Sci. Technol. A* **1994,** *12,* 2410-2414.

82. Jung, D. R.; Czanderna, A. W. Metal Overlayers on Organic Functional-Groups of Self-Organized Molecular Assemblies .3. X-Ray Photoelectron-Spectroscopy of Cr/Cn on 12-Mercaptododecanenitrile and of Cr/Ch3 on Octadecanethiol at Sample Temperatures from 173 to 373-K. *J. Vac. Sci. Technol. A* **1994,** *12,* 2402-2409.

83. King, D. E.; Czanderna, A. W. Oxidation Behavior of Thin Copper-Films on A Mercaptoundecanoic Acid Organized Molecular Assembly. *Langmuir* **1994,** *10,* 1630-1631.

84. Herdt, G. C.; Jung, D. R.; Czanderna, A. W. Weak interactions between deposited metal overlayers and organic functional groups of self-assembled monolayers. *Prog. Surf. Sci.* **1995,** *50,* 103-129.

85. Herdt, G. C.; Czanderna, A. W. Metal Overlayers on Organic Functional-Groups of Self-Organized

Molecular Assemblies .5. Ion-Scattering Spectroscopy and X-Ray Photoelectron-Spectroscopy of Ag/Cooh Interfaces. *J. Vac. Sci. Technol. A* **1995,** *13,* 1275-1280.

86. Jung, D. R.; Czanderna, A. W. Metal Overlayers on Organic Functional-Groups of Self-Assembled Monolayers .6. X-Ray Photoelectron-Spectroscopy of Cr/Cooh on 16-Mercaptohexadecanoic Acid. *J. Vac. Sci. Technol. A* **1995,** *13,* 1337-1344.

87. Jung, D. R.; Czanderna, A. W. Chemical and Physical Interactions at Metal/Self-Assembled Organic Monolayer Interfaces. *Crit. Rev. Solid. State. Mater. Sci.* **1994,** *19,* 1-55.

88. Konstadinidis, K.; Zhang, P.; Opila, R. L.; Allara, D. L. An In-Situ X-Ray Photoelectron Study of the Interaction Between Vapor-Deposited Ti Atoms and Functional-Groups at the Surfaces of Self-Assembled Monolayers. *Surf. Sci.* **1995,** *338,* 300-312.

89. Jung, D. R.; Czanderna, A. W. X-ray photoelectron spectroscopy of Cr/COOCH3 interfaces on self-assembled monolayers of 16-mercaptohexadecanoate. *Appl. Surf. Sci.* **1996,** *99,* 161-168.

90. Jung, D. R.; Czanderna, A. W.; Herdt, G. C. Interactions and penetration at metal/self-assemble organic monolayer interfaces. *J. Vac. Sci. Technol. A* **1996,** *14,* 1779-1787.

91. Herdt, G. C.; Jung, D. R.; Czanderna, A. W. Penetration of deposited Ag and Cu overlayers through alkanethiol self-assembled monolayers on gold. *Journal of Adhesion* **1997,** *60,* 197-222.

92. Herdt, G. C.; King, D. E.; Czanderna, A. W. Penetration of deposited Au, Cu, and Ag overlayers through alkanethiol self-assembled monolayers on gold or silver. *Zeitschrift fur Physikalische Chemie-International Journal of Research in Physical Chemistry & Chemical Physics* **1997,** *202,* 163-196.

93. Herdt, G. C.; Czanderna, A. W. Metal overlayers on organic functional groups of self-organized molecular assemblies .7. Ion scattering spectroscopy and x-ray photoelectron spectroscopy of Cu/CH3 and Cu/COOCH3. *J. Vac. Sci. Technol. A* **1997,** *15,* 513-519.

94. Herdt, G. C.; Czanderna, A. W. Metal overlayers on organic functional groups of self-assembled monolayers: VIII. X-ray photoelectron spectroscopy of the Ni/COOH interface. *J. Vac. Sci. Technol. A* **1999,** *17,* 3415-3418.

95. Dake, L. S.; King, D. E.; Czanderna, A. W. Ion scattering and X-ray photoelectron spectroscopy of copper overlayers vacuum deposited onto mercaptohexadecanoic acid self-assembled monolayers. *Solid State Sciences* **2000,** *2,* 781-789.

96. Jeon, N. L.; Nuzzo, R. G.; Xia, Y. N.; Mrksich, M.; Whitesides, G. M. Patterned Self-Assembled Monolayers Formed by Microcontact Printing Direct Selective Metalization by Chemical-Vapor-Deposition on Planar and Nonplanar Substrates. *Langmuir* **1995,** *11,* 3024-3026.

97. Jeon, N. L.; Clem, P. G.; Payne, D. A.; Nuzzo, R. G. A monolayer-based lift-off process for patterning chemical vapor deposition copper thin films. *Langmuir* **1996,** *12,* 5350-5355.

98. Jeon, N. L.; Lin, W. B.; Erhardt, M. K.; Girolami, G. S.; Nuzzo, R. G. Selective chemical vapor deposition of platinum and palladium directed by monolayers patterned using microcontact printing. *Langmuir* **1997,** *13,* 3833-3838.

99. SondagHuethorst, J. A. M.; Fokkink, L. G. J. Galvanic copper deposition on thiol-modified gold electrodes. *Langmuir* **1995,** *11,* 4823-4831.

100. Gilbert, S. E.; Cavalleri, O.; Kern, K. Electrodeposition of Cu nanoparticles on decanethiol-covered Au(111) surfaces: An in situ STM investigation. *J. Phys. Chem.* **1996,** *100,* 12123-12130.

101. Grummt, U. W.; Geissler, M.; SchmitzHuebsch, T. Chemical deposition of silver nanoclusters on self-assembled organic monolayers. A strategy to contact individual molecules. *Chem. Phys. Lett.* **1996,** *263,* 581-584.

102. Cavalleri, O.; Gilbert, S. E.; Kern, K. Electrochemical Cu deposition on thiol covered Au(111) surfaces. *Surf. Sci.* **1997,** *377,* 931-936.

103. Nishizawa, M.; Sunagawa, T.; Yoneyama, H. Underpotential deposition of copper on gold electrodes through self-assembled monolayers of propanethiol. *Langmuir* **1997,** *13,* 5215-5217.

104. Cavalleri, O.; Kind, H.; Bittner, A. M.; Kern, K. Temperature-promoted electrodeposition on thiolate-modified electrodes. *Langmuir* **1998,** *14,* 7292-7297.

105. Grummt, U. W.; Geissler, M.; Drechsler, T.; Fuchs, H.; Staub, R. An STM study of chemically deposited silver nanoclusters on mixed self-assembled monolayers. *Angewandte Chemie-International Edition* **1998,** *37,* 3286-3289.

106. Kind, H.; Bittner, A. M.; Cavalleri, O.; Kern, K.; Greber, T. Electroless deposition of metal nanoislands on aminothiolate-functionalized Au(111) electrodes. *J. Phys. Chem. B* **1998,** *102,* 7582-7589.

107. Oyamatsu, D.; Nishizawa, M.; Kuwabata, S.; Yoneyama, H. Underpotential deposition of silver

onto gold substrates covered with self-assembled monolayers of alkanethiols to induce intervention of the silver between the monolayer and the gold substrate. *Langmuir* **1998,** *14*, 3298-3302.

108. Hagenstrom, H.; Schneeweiss, M. A.; Kolb, D. M. Modification of a Au(111) electrode with ethanethiol. 1. Adlayer structure and electrochemistry. *Langmuir* **1999,** *15*, 2435-2443.

109. Hagenstrom, H.; Schneeweiss, M. A.; Kolb, D. M. Copper underpotential deposition on ethanethiol-modified Au(111) electrodes: kinetic effects. *Electrochim. Acta* **1999,** *45*, 1141-1145.

110. Hagenstrom, H.; Schneeweiss, M. A.; Kolb, D. M. Modification of a Au(111) electrode with ethanethiol. 2. Copper electrodeposition. *Langmuir* **1999,** *15*, 7802-7809.

111. Oyamatsu, D.; Kuwabata, S.; Yoneyama, H. Underpotential deposition behavior of metals onto gold electrodes coated with self-assembled monolayers of alkanethiols. *Journal of Electroanalytical Chemistry* **1999,** *473*, 59-67.

112. Esplandiu, M. J.; Hagenstrom, H.; Kolb, D. M. Functionalized self-assembled alkanethiol monolayers on Au(111) electrodes: 1. Surface structure and electrochemistry. *Langmuir* **2001,** *17*, 828-838.

113. Hagenstrom, H.; Esplandiu, M. J.; Kolb, D. M. Functionalized self-assemble alkanethiol monolayers on Au(111) electrodes: 2. Silver electrodeposition. *Langmuir* **2001,** *17*, 839-848.

114. Ekeroth, J.; Konradsson, P.; Bjorefors, F.; Lundstrom, I.; Liedberg, B. Monitoring the interfacial capacitance at self-assembled phosphate monolayers on gold electrodes upon interaction with calcium and magnesium. *Anal. Chem.* **2002,** *74*, 1979-1985.

115. Epple, M.; Bittner, A. M.; Kuhnke, A.; Kern, K.; Zheng, W. Q.; Tadjeddine, A. Alkanethiolate reorientation during metal electrodeposition. *Langmuir* **2002,** *18*, 773-784.

116. Doescher, M. S.; Tour, J. M.; Rawlett, A. M.; Myrick, M. L. Stripping voltammetry of Cu overlayers deposited on self-assembled monolayers: Field emission of electrons through a phenylene ethynylene oligomer. *J. Phys. Chem. B* **2001,** *105*, 105-110.

117. Ohgi, T.; Sheng, H. Y.; Nejoh, H. Au particle deposition onto self-assembled monolayers of thiol and dithiol molecules. *Appl. Surf. Sci.* **1998,** *132*, 919-924.

118. Ohgi, T.; Sheng, H. Y.; Dong, Z. C.; Nejoh, H. Observation of Au deposited self-assembled monolayers of octanethiol by scanning tunneling microscopy. *Surf. Sci.* **1999,** *442*, 277-282.

119. Ohgi, T.; Sheng, H. Y.; Dong, Z. C.; Nejoh, H.; Fujita, D. Charging effects in gold nanoclusters grown on octanedithiol layers. *Appl. Phys. Lett.* **2001,** *79,* 2453-2455.

120. Ohgi, T.; Fujita, D.; Deng, W.; Dong, Z. C.; Nejoh, H. Scanning tunneling microscopy and X-ray photoelectron spectroscopy of silver deposited octanethiol self-assembled monolayers. *Surf. Sci.* **2001,** *493,* 453-459.

121. Ohgi, T.; Fujita, D. Consistent size dependency of core-level binding energy shifts and single-electron tunneling effects in supported gold nanoclusters. *Phys. Rev. B* **2002,** *66*.

122. Ohgi, T.; Fujita, D. Single electron charging effects in gold nanoclusters on alkanedithiol layers with different molecular lengths. *Surf. Sci.* **2003,** *532,* 294-299.

123. Esplandiu, M. J.; Noeske, P. L. M. XPS investigations on the interactions of 1,6-hexanedithiol/Au(111) layers with metallic and ionic silver species. *Appl. Surf. Sci.* **2002,** *199,* 166-182.

124. Unger, W. E. S.; Lippitz, A.; Gross, T.; Friedrich, J. F.; Woll, C.; Nick, L. The use of octadecyltrichlorosilane self-assembled layers as a model for the assessment of plasma treatment and metallization effects on polyolefins. *Langmuir* **1999,** *15,* 1161-1166.

125. Huang, X. H.; Huang, H. Z.; Wu, N. Z.; Hu, R. S.; Zhu, T.; Liu, Z. F. Investigation of structure and chemical states of self-assembled - Au nanoscale particles by angle-resolved X-ray photoelectron spectroscopy. *Surf. Sci.* **2000,** *459,* 183-190.

126. Krishnamoorthy, A.; Chanda, K.; Murarka, S. P.; Ramanath, G.; Ryan, J. G. Self-assembled near-zero-thickness molecular layers as diffusion barriers for Cu metallization. *Appl. Phys. Lett.* **2001,** *78,* 2467-2469.

127. Hu, M.; Noda, S.; Tsuji, Y.; Okubo, T.; Yamaguchi, Y.; Komiyama, H. Effect of interfacial interactions on the initial growth of Cu on clean SiO2 and 3-mercaptopropyltrimethoxysilane-modified SiO2 substrates. *J. Vac. Sci. Technol. A* **2002,** *20,* 589-596.

128. Ganesan, P. G.; Cui, G.; Ellis, A. V.; Kane, R. S.; Ramanath, G. Near-zero-thickness self-assembled molecular layers for future device structures: Interfacial adhesion and diffusion barrier properties. *Thermec'2003, Pts 1-5* **2003,** *426-4,* 3487-3492.

129. Colavita, P. E.; Doescher, M. S.; Molliet, A.; Evans, U.; Reddic, J.; Zhou, J.; Chen, D.; Miney, P. G.; Myrick, M. L. Effects of metal coating on self-assembled monolayers on gold. 1. copper on

dodecanethiol and octadecanethiol. *Langmuir* **2002,** *18,* 8503-8509.

130. Wang, B.; Xiao, X. D.; Sheng, P. Growth and characterization of Au clusters on alkanethiol self-assembled monolayers. *J. Vac. Sci. Technol. B* **2000,** *18,* 2351-2358.

131. Wohlfart, P.; Weiss, J.; Kashammer, J.; Kreiter, M.; Winter, C.; Fischer, R.; Mittler-Neher, S. MOCVD of aluminum oxide/hydroxide onto organic self-assembled monolayers. *Chemical Vapor Deposition* **1999,** *5,* 165-170.

132. Fisher, G. L.; Hooper, A.; Opila, R. L.; Jung, D. R.; Allara, D. L.; Winograd, N. The interaction between vapor-deposited Al atoms and methylester-terminated self-assembled monolayers studied by time-of-flight secondary ion mass spectrometry, X-ray photoelectron spectroscopy and infrared reflectance spectroscopy. *J. Electron Spectrosc. Relat. Phenom.* **1999,** *99,* 139-148.

133. Hooper, A.; Fisher, G. L.; Konstadinidis, K.; Jung, D.; Nguyen, H.; Opila, R.; Collins, R. W.; Winograd, N.; Allara, D. L. Chemical effects of methyl and methyl ester groups on the nucleation and growth of vapor-deposited aluminum films. *J. Am. Chem. Soc.* **1999,** *121,* 8052-8064.

134. Fisher, G. L.; Hooper, A. E.; Opila, R. L.; Allara, D. L.; Winograd, N. The interaction of vapor-deposited Al atoms with CO2H groups at the surface of a self-assembled alkanethiolate monolayer on gold. *J. Phys. Chem. B* **2000,** *104,* 3267-3273.

135. Fisher, G. L.; Walker, A. V.; Hooper, A. E.; Tighe, T. B.; Bahnck, K. B.; Skriba, H. T.; Reinard, M. D.; Haynie, B. C.; Opila, R. L.; Winograd, N.; Allara, D. L. Bond insertion, complexation, and penetration pathways of vapor-deposited aluminum atoms with HO- and CH3O-terminated organic monolayers. *J. Am. Chem. Soc.* **2002,** *124,* 5528-5541.

136. Tour, J. M.; Kozaki, M.; Seminario, J. M. *J. Am. Chem. Soc.* **1998**, *120*, 8486.

137. Ratner, M. A.; Davis, B.; Kemp, M.; Mujica, V.; Roitberg, A.; Yaliraki, S. *Ann. N. Y. Acad. Sci.* **1998**, *852*, 22.

138. Collier, C. P.; Mattersteig, G.; Wong, E. W.; Luo, Y.; Beverly, K.; Sampaio, J.; Raymo, F. M.; Stoddart, J. F.; Heath, J. R. *Science* **2000**, *289*, 1172.

139. Zhou, C.; Deshpande, M. R.; Reed, M. A.; Jones, L., II; Tour, J. M. *Appl. Phys. Lett.* **1997**, *71*, 611.

140. Dhirani, A.; Lin, P.-H.; Guyot-Sionnest, P.; Zehner, R. W.; Sita, L. R. *J. Chem. Phys.* **1997**, *106*, 5249.

141. Metzger, R. M.; Chen, B.; Höpfner, U.; Lakshmikantham, M. V.; Vuillaume, D.; Kawai, T.; Wu, X.; Tachibana, H.; Hughes, T. V.; Sakurai, H.; Baldwin, J. W.; Hosch, C.; Cava, M. P.; Brehmer, L.; Ashwell, G. J. *J. Am. Chem. Soc.* **1997**, *119*, 10455.

142. Metzger, R. M.; Baldwin, J. W.; Shumate, W. J.; Peterson, I. R.; Mani, P.; Mankey, G. J.; Morris, T.; Szulczewski, G.; Bosi, S.; Prato, M.; Comito, A.; Rubin, Y. *J. Phys. Chem. B* **2003**, *107*, 1021.

143. Chen, J.; Reed, M. A.; Rawlett, A. M.; Tour, J. M. *Science* **1999**, *286*, 1550.

144. Chen, J.; Wang, W.; Reed, M. A.; Rawlett, A. M.; Price, D. W.; Tour, J. M. *Appl. Phys. Lett.* **2000**, *77*, 1224.

145. Reed, M. A.; Chen, J.; Rawlett, A. M.; Price, D. W.; Tour, J. M. *Appl. Phys. Lett.* **2001**, *78*, 3735.

146. Liang, W.; Shores, M. P.; Bockrath, M.; Long, J. R.; Park, H. *Nature* **2002**, *417*, 725.

147. Wacker, D.; Weiss, K.; Kazmaier, U.; Woll, C. Realization of a phenyl-terminated organic surface and its interaction with chromium atoms. *Langmuir* **1997,** *13*, 6689-6696.

148. Murty, K. V. G. K.; Venkataramanan, M.; Pradeep, T. Self-assembled monolayers of 1,4-benzenedimethanethiol on polycrystalline silver and gold films: An investigation of structure, stability, dynamics, and reactivity. *Langmuir* **1998,** *14*, 5446-5456.

149. Venkataramanan, M.; Murty, K. V. G. K.; Pradeep, T.; Deepali, W.; Vijayamohanan, K. Metal ion reactivity with 1,4-benzenedimethanethiol monolayers on gold. *Langmuir* **2000,** *16*, 7673-7678.

150. Oyamatsu, D.; Kanemoto, H.; Kuwabata, S.; Yoneyama, H. Nanopore preparation in self-assembled monolayers of alkanethiols with use of the selective desorption technique assisted by underpotential deposition of silver and copper. *Journal of Electroanalytical Chemistry* **2001,** *497*, 97-105.

151. Ahn, H.; Whitten, J. E. Vapor-deposition of aluminum on thiophene-terminated self-assembled monolayers on gold. *J. Phys. Chem. B* **2003,** *107*, 6565-6572.

Chapter 2

Solvation of Zero-Valent Metals in Organic Thin Films

Abstract: Aluminum, copper and silver atoms are found to form a weakly solvated quasi-isotropic layer when vapor-deposited onto methoxy groups exposed at the surface of a hexadecanethiolate self-assembled monolayer on Au {111}. The nature of the interactions was revealed using SIMS, XPS and IRS, and supported by DFT calculations. This method complements 3-dimensional gas phase cluster experiments by providing an approach for controlling solvation geometry and bonding via the molecular parameters of the monolayer. The results are discussed in terms of their applicability to the design of controlled interfaces, particularly metal contacts in molecular electronic devices.

1. Introduction

The interaction of metals with organic functional groups in thin films is important in a number of areas including organometallic chemistry, polymer chemistry and more recently to the growing field of molecular electronics. For example, the study of the reactivity of zero-valent metal atoms with molecular solvents comprises an important part of organometallic chemistry [1-6]. Details of the solvent-metal interactions are sparse since it is difficult to prepare solutions of isolated metal atoms in typical solvents, e.g. alkyl ethers. A limited amount of data is available from gas-phase studies of solvated clusters and matrix isolation experiments [2-6]. Such experiments, while very informative in terms of solvation energetics and electron transfer properties, are not yet able to provide a complete picture of the structural geometry and bonding. The interaction of metals with polymer thin films also has been extensively examined at least in part due to the obvious technical applications. A central result of these studies on polymer films is the weakness of the interactions between various metal atoms, deposited from the vapor phase, and the polymer [7-9]. However, since it is difficult to ascertain the exact composition and structure of polymer surfaces, it has not yet been possible to elucidate the nature of the bonding that leads to such weak interactions.

In this letter, we report on the use of self-assembled monolayers (SAMs) to reveal heretofore inaccessible details of the metal-organic functional group interaction. These materials provide a unique template for these studies since it is possible to prepare surfaces with a wide variety of terminal group functionalities, composition and topographic configurations. The details of the bonding can be revealed using a combination of surface science probes. In this study we have employed time-of-flight

secondary ion mass spectrometry (ToF SIMS), X-ray photoelectron spectroscopy (XPS) and infrared spectroscopy (IRS). The concept is illustrated by examining the interaction of Al, Cu and Ag atoms on the surface of a methoxy-terminated hexadecanethiolate SAM on gold, and is a model for the interaction of metal atoms with alkyl ether solvent molecules. The results show that these metal atoms interact with the methoxy terminal group forming a weakly solvating, quasi-isotropic layer. Concomitant theoretical calculations reveal the importance of orientational effects and provide additional insight into the detailed nature of the bonding. We recognize the applicability of this novel construct for the creation of highly controlled metal-organic interfaces. An important example is the control of the metal contacts in a variety of molecular electronic devices since the interaction is weak enough to allow the identity of the surface functional groups to be maintained, yet strong enough to provide an unimpeded path to electron flow.

2. Experimental

2.1 SAM Preparation and Analysis

The preparation and characterization of the types of SAMs used in this study has been described in detail previously [10,11]. Briefly, self-assembly of well-organized monolayers was achieved by immersing the Au substrates into millimolar solutions of the SAM molecules in absolute ethanol for ~2 days at ambient temperature. The monolayer films were characterized with single wavelength ellipsometry, infrared spectroscopy and contact angle measurements to ensure that they were densely packed with clean surfaces.

In all cases, the metals (Al, Cu and Ag; Goodfellow, R.D. Mathis, Alfa Aesar ≥ 99.995 %) were thermally evaporated at a rate of ~0.15 atoms·nm^{-2}·s^{-1} as measured by a

quartz crystal microbalance (QCM). Samples were kept in vacuum continuously during deposition and analysis.

The ToF-SIMS analyses were performed on a custom designed instrument as described previously [12]. Briefly, the instrument consists of a loadlock, a preparation chamber, a metal deposition chamber and the primary analysis chamber, each separated by a gate valve. The primary Ga^+ ions were accelerated to 15 keV and contained in a 100 nm diameter probe beam which was rastered over a (106x106) μm^2 area during data acquisition. All spectra were acquired using a total ion dose of less than 10^{11} ions·cm^{-2}. Relative peak intensities are reproducible to within ± 8 % from sample to sample and ± 8 % from scan to scan.

Infrared analyses were performed on a Fourier transform instrument (Mattson Research Series 1000) fitted with custom in-house optics configured external to the instrument and designed for grazing incidence reflection of samples under vacuum [10]. A liquid nitrogen cooled MCT detector was used with an effective low frequency cutoff of ~750 cm^{-1}.

The XPS analyses were performed on a spectrometer (Scienta ESCA 300) equipped with a monochromatic Al K_α source, as described in detail elsewhere [13,14]. A pass energy of 75 eV and an energy step of 0.05 eV was used for the analysis. The resulting full width at half maximum (FWHM) for Au $4f_{7/2}$ is 0.52 eV. A binding energy of 84.00 eV for Au $4f_{7/2}$ was used as a reference for all spectra.

2.2 Ab-Initio Quantum Calculations

Density Functional Theory (DFT) calculations were performed to provide estimates of the interactions of the metal atoms - Al, Cu, and Ag - and the methoxy group of the

SAM. Calculations were carried out using the algorithms available in the Gaussian 98 Rev. A.9 program package [15].

Interactions between SAM terminal groups and metal atoms can range from Van der Waals to weakly electrostatic to covalent [16]. To accurately determine these binding energies, small model systems were chosen to allow the use of larger basis sets and various different starting geometries which would prove too computationally expensive if the entire alkanethiolate complex was used. Therefore the calculations were carried out on the simple isolated systems M + CH_3OCH_3 and $CH_3CH_2CH_3$, where M = Al, Cu, Ag. The most extensive results were obtained for Al atom complexes since the smaller number of electrons in comparison to Cu, Ag and Au allowed the use of larger basis sets. Geometry optimizations for these Al model systems were performed at using the B3PW91 functional with the 6-311+G(2df,p) and the LANL2DZ basis sets. Aluminum interaction energies using the B3PW91/6-311+G(2df,p) level of theory compare well to those calculated for Al with water [17,18] and dimethyl ether [19] using MP, quadratic configuration interaction (QCI) and CC methodologies [17-19] and experimentally derived values [20,21]. The Au, Ag, and Cu complexes were run solely at the B3PW91/LAN2DZ level since the heavier metals require the use of effective core potentials (ECPs) to reduce the computational cost of the large number of electrons present in each atom. The use of ECPs has been shown by several groups to compare well with full electron calculations in the case of several small Au-, Ag-, and Cu-containing molecules [22,23]. The interaction energy of the model system with Al, Cu, and Ag were determined by relative energy of the geometry-optimized complex with

respect to the energies of the optimized components. Additionally, thermal and zero point energy corrections were obtained from frequency calculations.

2.3 Definition of Deposited Metal Coverage

For ease in data analysis and interpretation, the deposited amounts were converted to coverage of metal atoms per SAM molecule, designated θ_M (M = Al, Cu, Ag). The SAM molecular density is 4.6 molecules nm^{-2} in a well-formed alkanethiolate / Au{111} SAM [24]. Thus for $\theta_M = 1.0$ there would be one metal atom deposited on average per SAM molecule. In all data analysis we assume that the sticking probability of the deposited metal atoms is unity on the SAM monolayer. We assume the sticking probability is near unity based upon comparison to XPS metal intensities with expected values obtained from the QCM. Moreover, in the SIMS experiments, metal signals are observed synchronously with the onset of metal deposition.

3. Results and Discussion

The terminal group interaction with deposited Ag observed by time-of-flight secondary ion mass spectrometry (ToF SIMS), X-ray photoelectron spectroscopy (XPS) and infrared reflection spectroscopy (IRS) are displayed in figure 1. Upon deposition of Ag from the vapor phase on the $–OCH_3$ terminated SAM, a portion of the Ag atoms are found to penetrate to the Au/S interface and the remainder interact with the methoxy terminal group. Penetration of the A1 and Cu atoms to the Au/S interface is also observed. For Cu and Ag, metal atom penetration continues at all metal coverages, whereas for Al, penetration of the metal atoms ceases after a 1:1 Al:Au ratio is achieved [10,25]. Penetration is uniquely correlated with the appearance of $Au_xMetal_yS_z$ cluster ions observed by SIMS [10,25]. In the positive ion SIMS spectrum, the intensity of the

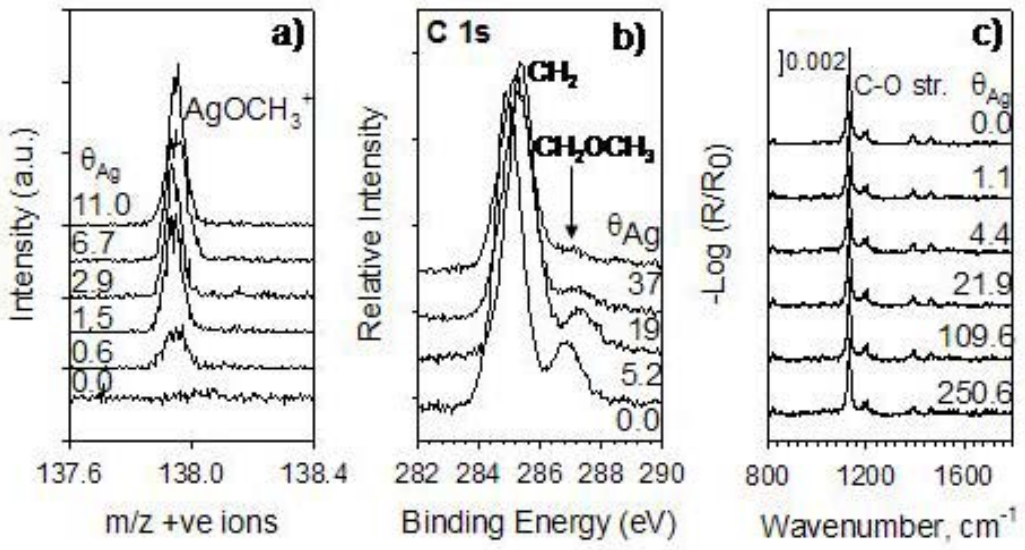

Figure 1. (a) . High mass resolution positive ion SIMS spectra of $AgOCH_3^+$ fragments, nominal mass 138 Da. (b) XPS spectrum of C1s region of methoxy-terminated SAM upon deposition of Ag (c) Low frequency IRS spectra of the methoxy-terminated SAM upon deposition of Ag. q_{Ag} is defined as the number of deposited Ag atoms per SAM molecule. Samples were kept in vacuum continuously during deposition and analysis.

$AgOCH_3^+$ (m/z = 138) peak is shown for increasing values of θ_{Ag} (Figure 1a). No $Ag_XO_Y^{\pm}$ ions are observed.

Based on our previous work [26,27] with –COOH and $–CO_2CH_3$ terminated SAMS, the appearance of $AgOCH_3^+$ but not $Ag_XO_Y^{\pm}$ ions indicates that the deposited Ag has not undergone an insertion reaction with $–OCH_3$ to form Ag-O bonds but suggests that a weak organo-silver complex has formed. Furthermore, upon deposition of Al and Cu, $MOCH_3^+$ ions rather than $M_XO_Y^{\pm}$ ions are observed, where M = Al, Cu, indicating that for these metals weak organo-metallic complexes have also formed.

The C1s peaks from the XPS spectra at 286.8 eV and 284.9 eV are assigned to the $–\underline{\mathbf{C}}H_2O\underline{\mathbf{C}}H_3$ C atoms and the $–(\underline{\mathbf{C}}H_2)-$ alkyl chain respectively as shown in figure 1b. Upon deposition of Ag, the $–\underline{\mathbf{C}}H_2O\underline{\mathbf{C}}H_3$ peak vanishes by $\theta_{Ag} \leq 37$ Ag atoms/SAM molecule. At the same time, the $–(\underline{\mathbf{C}}H_2)-$ C1s peak broadens and shifts to a slightly higher binding energy (285.3 eV). For Al, the $–\underline{\mathbf{C}}H_2O\underline{\mathbf{C}}H_3$ peak also disappears by $\theta_{Al} \leq 1.3$ Al atoms/SAM molecule. These data indicate that on average there is a ~1:1 perturbing interaction between the metal and the $–OCH_3$ group that shifts the $–\underline{\mathbf{C}}H_2O\underline{\mathbf{C}}H_3$ binding energy to lower values merging it into the main $–(\underline{\mathbf{C}}H_2)-$ C1s peak. Further evidence of the Ag and Al interaction with the terminal group is given by the O1s spectrum (data not shown).

Perhaps the clearest evidence for the absence of Ag insertion into the $–OCH_3$ group is given by the nearly constant character of the C-O stretching mode at 1132 cm^{-1} in the IRS spectra at all Ag coverages (Figure 1c). The δ_{CH3} (CH_3 def., 1383 cm^{-1}) and δ_{CH2} (CH_2 scissor, 1468 cm^{-1}) modes are also virtually unaffected by the deposition of Ag atoms. Taken together, these data indicate that there is no significant chemical

interaction between the deposited Ag and the $–OCH_3$ terminated SAM. Similar behavior is found for Cu and Al deposition. Moreover, an Al-O stretch in the vicinty of ~855 cm^{-1} is not observed confirming that there has been no bond cleavage at the methoxy terminal group.

Hence, the experimental data point to the formation of a weak $M...OCH_3$ complex, where M = Al, Cu and Ag, and rule out insertion of the metal atom into the C-O bond. Note the subtly of the interaction: weak enough to cause little disturbance of the C-O stretching mode but strong enough to perturb the local electron density such that the C1s binding energy shifts to lower binding energies.

To further quantify the interaction quantum mechanical calculations of isolated model systems, M + CH_3OCH_2 and $CH_3CH_2CH_3$, where M = Al, Cu, Ag, were performed. For Ag and Cu insertion into the C-O bond, the calculations fail to converge indicating that the structure is unstable. Moreover, insertion of Ag and Cu into the C-C bond is unstable by 142 and 49 kJ mol^{-1} respectively and would not be observed, in agreement with our observations. In contrast, for the Al system, the lowest energy configuration, -272 kJ mol^{-1}, is the *insertion* of the Al into the C-O bond with a secondary minimum, -90 kJ mol^{-1}, for insertion into the C-C bond. Since neither of these processes is observed experimentally, we assume that the activation barriers are prohibitively high.

However, there are secondary energy minima for all these systems for the stabilization of the metal atom [10,25] adjacent to O by -33 kJ mol^{-1} for Al, -34 kJ mol^{-1} for Cu and –13 kJ mol^{-1} for Ag whilst there is no preference for the metal atom to be isolated or adjacent to the hydrocarbon. Thus, there is a preference for the metal atoms to be located close to the O atom rather than the C atom of the methoxy group.

The minimum energy configuration for all the metal atoms is behind the O atom, away from the C-O bonds. Simple geometric considerations for the interaction of the SAM with the metal atom (figure 2) show that the isolated atom geometry will be unfavorable due to steric hindrances at the SAM/vacuum interface. While a small fraction of the methoxy groups may be able to reorient to allow ideal metal-oxygen interactions, most $–OCH_3$ groups will not due to intermolecular repulsion forces. Thus we expect that the average stabilization energy per metal atom will be significantly reduced in the SAM case relative to the isolated system. This is in qualitative agreement with the observed behavior of the C-O stretch mode, which remains essentially unchanged upon metal deposition.

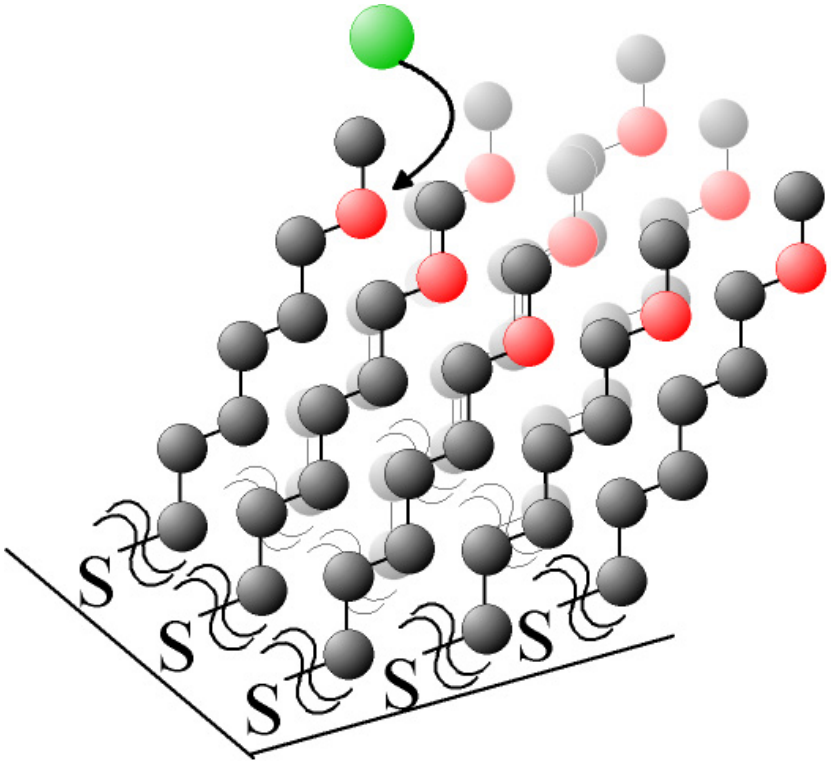

Figure 2. Schematic illustration showing the steric hindrance of the metal oxygen atom. The metal atom is represented by the green sphere, oxygen atom is red and hydrocarbon moieties are black.

At room temperature, the methoxy group has a large number of configurations due to the low rotational energy barriers of the alkyl C-O bond relative to the C-C bond. There will be a wide range of configurations of metal atoms analogous to a weakly solvating, quasi-isotropic layer. We therefore view the interaction between these Al, Cu or Ag atoms and the methoxy terminal group as a "solvation" rather than a complexation with a directed interaction and a specific geometry. These experiments complement studies of solvation and electron transfer reactions of metal atoms with gas-phase molecules and clusters. In our experiments, whilst the underlying metal atom – molecular group interactions remain the same, the reaction is constrained to a quasi-planar configuration compared to the 3D geometry in the gas phase experiment.

The ability to have such fine control of bonding interactions at metal – organic interfaces has important applications in the fabrication and design of top metal contacts for molecular electronics. In these applications, the fine control of metal – molecule bonding, ranging from no electronic overlap of states to complete chemical degradation, is critical in optimizing device performance [28].

4. Conclusions

We have shown that with multiple surface science techniques, metal deposition on SAMS reveals the presence of weak metal–organic group interactions with high sensitivity. By constraining the interaction to a quasi-planar configuration, rather than 3D geometry in a gas phase experiment, we are able to exploit properties such as steric hindrance, in addition to metal reactivity, and thus tune the properties of the metal – SAM system. This strategy has allowed us to observe solvation states for a number of metals in a

controlled steric environment and points to new applications for these types of systems from designing new metallic contacts for organic electronic devices to catalysis.

5. Acknowledgements

The authors acknowledge financial support from the Office of Naval Research and the National Science Foundation.

6. References

1. K.J. Klabunde, in: R.A. Abramovitch (Ed.), Reactive Intermediates Vol. 1, Plenum Press, New York, 1980
2. P. Kasai, J. Phys. Chem. A 106 (2002) 83
3. D.B. Pederson, M.Z. Zgierski, S. Anderson, D.B.Rayner, B. Simard, S. Li, D.-S. Yang, J. Phys. Chem. A 105 (2001) 11462
4. C.P.Schulz, C. Nitsch, J. Chem. Phys.107 (1997) 9794
5. J.J. Carroll, J.C. Weisshaar, J. Phys. Chem. 100 (1996) 12355
6. P.A. Willis, H.U. Stauffer, R.Z. Hinrichs, H.F. Davis, J. Chem. Phys. 108 (1998) 2665
7. J.J. Pireaux, Syn. Met. 67 (1994) 39
8. T. Strunksus, M. Grunze, G. Kochendoerfer, Ch. Wöll, Langmuir 12 (1996) 2712
9. F. Faupel, R. Willecke, A. Thran, Mater. Sci. Eng. R22 (1998) 1
10. G.L. Fisher, A.V. Walker, A.E. Hooper, T.B. Tighe, K.B. Bahnck, H.T. Skriba, M.D. Reinard, B.C. Haynie, R.L. Opila, N. Winograd, D.L. Allara, J. Am. Chem. Soc. 124 (2002) 5528
11. P.E. Laibinis, C.D. Bain, R.G. Nuzzo, G.M. Whitesides, J. Phys. Chem. 99 (1995) 7663
12. R.M. Braun, P. Blenkinsopp, S.J. Mullock, C. Corlett, K.F. Willey, J.C. Vickerman, N. Winograd, Rapid Commun. Mass. Spec. 12 (1998) 1246
13. G. Beamson, D. Briggs, S. F. Davies, I. W. Fletcher, D. T. Clark, J. Howard, U. Gelius, B. Wannberg, P. Balzer, Surf. Interface Anal. 15 (1990) 541

14. U. Gelius, B. Wannberg, P. Baltzer, H. Fellnerfeldegg, G. Carlsson, C. G. Johansson, J. Larsson, P. Munger, G. Vegerfors, J. Elec. Spec. Rel. Phenom. 52 (1990) 747

15. Gaussian 98, Revision A.9, M.J. Frisch, G.W. Trucks, H.B. Schlegel, G.E. Scuseria, M.A Robb, J.R. Cheeseman, V.G. Zakrzewski, J.A. Montgomery Jr, R.E. Stratmann, J.C. Burant, S. Dapprich, J.M. Millam, A.D. Daniels, K.N.O. Kudin, F.M.C. Strain, O. Farkas, J. Tomasi, V. Barone, M. Cossi, R. Cammi, B. Mennucci, C. Pomelli, C. Adamo, S. Clifford, J. Ochterski, G.A. Petersson, P.Y. Ayala, Q. Cui, K. Morokuma, D.K. Malick, A.D. Rabuck, K. Raghavachari, J.B. Foresman, J. Cioslowski, J.V. Ortiz, A.G. Baboul, B.B. Stefanov, G. Liu, A. Liashenko, P. Piskorz, I. Komaromi, R. Gomperts, R.L. Martin, D.J. Fox, T. Keith, M.A. Al-Laham, C.Y. Peng, A. Nanayakkara, M. Challacombe, P.M.W. Gill, B. Johnson, W. Chen, M.W. Wong, J.L. Andres, C. Gonzalez, M. Head-Gordon, E.S. Replogle, J.A. Pople, Gaussian Inc., Pittsburgh, PA, 1998

16. S. Sakai, J. Phys. Chem. 96 (1992) 8369

17. S. Sakai, J. Phys. Chem. 97 (1993) 8917

18. J. M. Parnis, S. A. Mitchell, D. M. Rayner, P.A. Hackett, J. Phys. Chem. 92 (1988) 3869.

19. F. S. Legge, G. L. Nyberg, J. B. Peel, J. Phys. Chem. A 105 (2001) 7905

20. J. M. Seminario, A. G. Zacarias, J. M. Tour, J. Phys. Chem. A 103 (1999) 7883

21. J. M. Seminario, A. G. Zacarias, J. M. Tour, J. Am. Chem. Soc.121 (1999) 411

22. D. B. Pedersen, M. Z. Zigierski, S. Anderson, D. M. Rayner, B. Simard, J. Phys. Chem A 105 (2001) 11462

23. T. Fängström, S. Lunell, P. H. Kasai, L. A. Eriksson, J. Phys. Chem. A 102 (1998) 1005

24. L.H. Dubois, R.G. Nuzzo, Ann. Rev. Phys. Chem. 43 (1992) 437

25. A.V. Walker, T.B. Tighe, O. Cabarcos, M.D. Reinard, L. Dake, B.C. Haynie, D.L. Allara, N. Winograd, in preparation

26. A. Hooper, G.L. Fisher, K. Konstadinidia, D. Jung, H. Nguyen, R. Opila, R.W. Collins, N. Winograd, D.L. Allara, J. Am. Chem. Soc. 121 (1999) 8052

27. G.L. Fisher, A.E. Hooper, R.L. Opila, D.L. Allara, N. Winograd, J. Phys. Chem. B 104 (2000) 3267

28. D.L. Allara, T.D. Dunbar, P.S. Weiss, L.A. Bumm, M.T. Cygan, J.M. Tour, W.A. Reinerth, Y. Yao, M. Kozaki, L. Jones, II, Ann. NY Acad. Sci. 852 (1998) 349

Chapter 3

The Dynamics of Metal Penetration Through Methoxy-Terminated Organic Monolayers

Abstract: We have studied the interaction of vapor-deposited Al, Cu, Ag and Au atoms with a methoxy-terminated self-assembled monolayer (SAM) of $HS(CH_2)_{16}OCH_3$ on polycrystalline Au{111}. Time-of-flight secondary ion mass spectrometry, infrared reflection spectroscopy and x-ray photoelectron spectroscopy measurements at increasing coverages of metal show that for Cu and Ag deposition at all coverages the metal atoms continuously partition into competitive paths: penetration through the SAM to the S/substrate interface and solvation-like interaction with the $-OCH_3$ terminal groups. Deposited Au atoms, however, undergo only continuous penetration, even at high coverages, leaving the SAM "floating" on the Au surface. These results contrast with previous ones on Al deposition where metal atom penetration to the Au/S interface ceases abruptly after a ~1:1 Al:Au layer has been attained. These observations are interpreted in terms of a thermally activated penetration mechanism involving dynamic formation of diffusion channels in the SAM via hopping of alkanethiolate-metal (RSM-) moieties across the surface. Using supporting quantum chemical calculations, the results are rationalized in terms of the relative heights of the hopping barriers, RSAl > RSAg, RSCu > RSAu, and the magnitudes of the metal-OCH_3 solvation energies.

1. Introduction

Understanding the atomic and molecular level interaction of metal atoms with organic surfaces is becoming increasingly important as the number of applications involving metal-organic interfaces grows. In addition to the longstanding general interest in metallization of polymers, [1-3] of particular interest recently has been the emergence of the fields of polymer and molecular electronic devices [4-16] in which the issue of optimizing top-metal contacts is of critical importance [17].Given the complexity of these structures in terms of chemical interactions and metal film morphology, and given the wide range of choices in metals, organic materials and deposition conditions, the rational design of metal/organic structures requires a broad, fundamental understanding of the mechanistic and thermodynamic aspects of metal atom-molecule interactions. The spectrum of interactions can be quite varied, ranging from weak adsorption, which could lead to clustering with poor adhesion and/or electrical contact and diffusion into the bulk, to strong chemical reaction with severe destruction of chemical integrity. Recent efforts to explore fundamental interactions have focused on the use of self-assembled monolayers (SAMs) because of their highly organized surface structures with uniform density of organic groups that allow quantitative characterization of the metal-molecule interactions [18-28]. This approach is directly relevant to molecular electronic devices whose core structures depend upon SAMs, typically with vacuum deposited metal contacts [7,14]. On a more fundamental level, these types of experiments add a new strategy to the study of organometallic chemistry by providing quantitative probes of nascent metal atom interactions with organic functional groups in well-defined geometries under highly controlled conditions. In particular, this strategy complements current studies of solvation

and electron transfer reactions of metal atoms with gas-phase molecules and clusters [29-31]. Of special significance in the metal-SAM experiments is the ability to control the orientations and spacing of the organic groups presented to the metal atoms, as opposed to the unconstrained geometries in the 3-D gas-phase experiments.

Recently our group has studied the interaction of vapor deposited Al atoms with a selected range of common O-containing groups including -CO_2CH_3 [26], -COOH [27], -OH [28] and -OCH_3 [28] along with control experiments on -CH_3 [26]. Aluminum was chosen as a metal because of its common use in microelectronics applications, its well-known organometallic chemistry with O-containing molecules [32] and our discovery that over the range of functional groups surveyed Al displays a wide range of chemical and physical interactions. The latter point is illustrated by the observations that vapor deposited Al can react to form organoaluminum complexes (-CO_2CH_3, -COOH and -OH), penetrate to the Au/S interface (-CH_3), or both penetrate to the Au/S interface and be weakly stabilized by the terminal group at the SAM/vacuum interface (-OCH_3) [28]. The Al metal atom penetration into the –CH_3 [26] and –OCH_3 [28] terminated SAMs was proposed to occur via thermally-activated lateral hopping of the S atom of the alkanethiolate from favorable Au adsorption sites, which leads to the creation of transient holes allowing transport of nearby Al atoms directly to the S/Au interface [26,28].

The case of the –OCH_3 terminated SAM [28] is of particular value since this group displays an intermediate reactivity between the limiting cases of –CH_3, where Al penetrates to the Au/S interface, and -COOH, -CO_2CH_3 and -OH cases, where Al interacts solely with the terminus. Thus, an -OCH_3 terminated SAM should be an ideal case for a study of the relationship between the detailed metal-molecule interactions at the vacuum interface and

variations in the metal atoms deposited. Since copper, gold, silver and aluminum are widely used in the microelectronics industry; this set of metals is of prime interest for such a study. Gold is primarily employed for ohmic contacts [33] while copper and silver are widely used for wiring [34]. Since the mid-1990s, copper has also been employed to inter-connect layers in microchips. This technology has started to supplant traditional aluminum metallization techniques [35].

In this paper we investigate the interaction of Ag, Cu and Au, deposited at room temperature from thermal sources, with a methoxy terminated SAM. Infrared reflection spectroscopy (IRS) and time-of-flight secondary-ion-mass-spectrometry (ToF-SIMS) are used as primary *in-situ* tools, along with x-ray photoelectron spectroscopy (XPS) to characterize the chemical and physical interactions of the metal atoms with the SAM as a function of varying metal atom coverage. The results show that under our experimental conditions deposited Cu and Ag atoms, independent of coverage, partition between solvation types of interactions with the $–OCH_3$ terminal groups [36] and penetration to the Au/S interface. In the case of Au deposition, however, no interaction with the terminal group is observed and the deposited metal atoms penetrate to the Au/S interface, independent of coverage. These results are compared with those obtained for Al interacting with the $–OCH_3$ terminated SAM in which the partitioning between stabilization at the $–OCH_3$ surface and penetration into the SAM ceases abruptly at ~1 Al deposited per Au surface atom [28]. Interpretation of these results is made on the basis of a general mechanism involving dynamic competitions between metal-molecule interactions and the rates of fluctuations of chain hopping controlled by the barrier heights of metal-thiolate diffusion.

2. Experimental

2.1. Materials and General Procedures

The preparation and characterization of SAMs used in this study has been described in detail previously [28,37-45]. The metals for all depositions were obtained from different sources (Goodfellow, R.D. Mathis, Alfa Aesar, Sigma Aldrich) but were of greater than 99.99 % purity in all cases.

2.2. SAM Preparation

Films of Cr (~5 nm) and Au (~200 nm) were thermally deposited sequentially onto clean Si(001) native oxide covered wafers. Self-assembly of well-organized monolayers was achieved by immersing the Au substrates into millimolar solutions of the relevant hexadecanethiol molecules in absolute ethanol for ~2 days at ambient temperature. The monolayer films were characterized with single wavelength ellipsometry, infrared spectroscopy and contact angle measurements to ensure that they were densely packed, clean surfaces. In addition, all SAMs were characterized by ToF-SIMS, XPS and IRS measurements prior to metal deposition.

2.3 Time-of-Flight Secondary Ion Mass Spectrometry

The ToF-SIMS analyses were performed on a custom designed instrument as described previously [46]. Briefly, the instrument consists of a loadlock, a preparation chamber, a metal deposition chamber and the primary analysis chamber, each separated by a gate valve. The primary Ga^+ ions were accelerated to 15 keV and contained in a 100 nm diameter probe beam which was rastered over a (106x106) μm^2 area during data acquisition. All spectra were acquired using a total ion dose of less than 10^{11} ions·cm^{-2}.

Relative peak intensities are reproducible to within ± 8 % from sample to sample and ± 8 % from scan to scan.

The metals were deposited onto the sample at room temperature from a W-wire basket source at a rate of ~0.15 atoms·nm^{-2}·s^{-1} with the pressure below 5x10^{-8} Torr. After deposition, the preparation chamber pressure was allowed to recover to the base value of 1.5x10^{-9} Torr before sample transfer to the analysis chamber. The deposited mass/area was monitored using a Maxtek, Inc. TM-400 quartz crystal microbalance (QCM) controller with a maximum error within ± 8 %.

2.4 Infrared Spectroscopy

Analyses were performed on a Fourier transform instrument (Mattson Research Series 1000) fitted with custom in-house optics configured external to the instrument and designed for grazing incidence reflection of samples under vacuum [26-28]. A liquid nitrogen cooled MCT detector was used with an effective low frequency cutoff of ~750 cm^{-1}. The infrared beam was allowed to access the vacuum system and reflect from the sample through a pair of differentially-pumped KBr windows. After analysis of the bare monolayer, a shield was moved to unblock the path between the sample and the metal source. The metals were evaporated from a W-wire basket at a rate of ~ 0.15 atoms·nm^{-2}·s^{-1} as measured by a QCM. The pressure remained below 1x10^{-7} Torr during the deposition.

2.4. X-Ray Photoelectron Spectroscopy

The XPS analyses were performed on a spectrometer (Scienta ESCA 300) equipped with a monochromatic Al K_α source, as described in detail elsewhere [47,48]. A pass energy of 75 eV and an energy step of 0.05 eV were used for the analysis. The resulting full width at

half maximum (FWHM) for Au $4f_{7/2}$ is 0.52 eV. A binding energy of 84.00 eV for Au $4f_{7/2}$ was used as a reference for all spectra.

Following analysis of the bare monolayer the sample was transferred under vacuum to the deposition chamber, which is isolated from the analysis chamber by a gate valve. The pressure in the preparation chamber remained below $5x10^{-8}$ Torr during the deposition. Incremental amounts of aluminum and silver were deposited at a highly controlled, constant rate, typically ~0.15 atoms·nm^{-2}·s^{-1} as monitored by a QCM, by evaporation from a graphite crucible heated to 1248 K and 1198 K respectively. After deposition the metal/SAM specimen was transferred directly under vacuum to the analysis chamber where the pressure was maintained below $1x10^{-8}$ Torr.

2.6 Quantum Chemistry Calculations

Density Functional Theory (DFT) calculations were performed to provide estimates of the interactions of Al, Cu, Ag and Au atoms with the $–OCH_3$ and –S– moieties of the molecules. All calculations were carried out using the Gaussian 98 Rev. A.9 program package [49].

In the case of the metal-S interactions the SAM molecule was truncated by 11 methylene units and modeled as CH_3O-$(CH_2)_5$-SH to reduce the computational cost. This simplification is not expected to significantly affect the calculated bond energies since intra-molecular induction effects typically range over 2-3 bonds. Geometry optimizations and frequency calculations were performed at the B3PW91/LANL2DZ level of theory. The LANL2DZ basis sets, which use an effective core potential (ECP), were used to reduce explicit consideration of the large number of electrons in the metal atoms. It has been demonstrated that calculations using ECPs compare well with full electron calculations in

the case of several small Au-, Ag-, and Cu- containing molecules [50] as well as in several S-Au species [51]. All energies are reported as enthalpies of the final structures relative to the isolated reactants and contain zero point energy corrections and thermal energy corrections for standard temperature and pressure.

For computational efficiency in achieving accurate interaction energies between the metal atoms and the $–OCH_3$ group, small model systems of M + CH_3OCH_3 and $CH_3CH_2CH_3$ were used, where M = Al, Cu, Ag and Au. The most accurate results were obtained for Al atom complexes since the smaller number of electrons in comparison to Cu, Ag and Au allowed the use of larger basis sets. Geometry optimizations for these Al model systems were performed at using the B3PW91 functional with the 6-311+G(2df,p) and the LANL2DZ basis sets. Aluminum interaction energies using the B3PW91/6-311+G(2df,p) level of theory compare well to those calculated for Al with water [52,53] and dimethyl ether [54] using MP, quadratic configuration interaction (QCI) and coupled cluster (CC) methodologies [52-54] and experimentally derived values [55]. The Au, Ag, and Cu complexes were run solely at the B3PW91/LANL2DZ level. The interaction energy of the model system with Al, Cu, Ag and Au were determined as the relative energy of the geometry-optimized complex with respect to the energies of the optimized components. Additionally, thermal and zero point energy corrections were obtained from frequency calculations.

2.7 Definition of Deposited Metal Coverage

The metal deposition onto the samples was monitored directly as the mass per unit area by a quartz crystal microbalance (QCM). For ease in data analysis and interpretation, the deposited amounts were converted to coverage of metal atoms per SAM molecule,

designated θ_M (M = Al, Cu, Ag, Au). The SAM molecular density is 4.6 molecules·nm^{-2} in a well-formed alkanethiolate on Au{111} [56]. Thus for θ_M = 1.0 there would be one metal atom deposited on average per SAM molecule.

3. Results

We note that the results for the deposition of Al on –OCH_3 terminated SAMS have been reported in detail in reference 28 and are included here for comparison purposes.

3.1 ToF SIMS

A detailed discussion of the positive and negative ion mass spectra of the bare –OCH_3 monolayer is given in reference 28. In agreement with previous work [26-28,57-60], we find that the relative intensities of Au_X^-, $Au_XS_Y^-$ and SO_Z^- (where z = 1-4) provide us with a useful indication that the SAM was prepared without substantial incorporation of impurities or oxidative products.

3.1.1 Deposition of Al, Cu and Ag

The positive ion mass spectra show evidence that the metal atoms interact with the terminal -OCH_3 group. Specifically, in Figure 1, the intensity of the $MOCH_3^+$ (m/z = 58, 94, 138 respectively) peaks, indicative of metal-OCH_3, increases for increasing values of θ_M, where M = Al, Cu, Ag. The $AlOCH_3^+$ and $CuOCH_3^+$ spectra are normalized to the initial peak intensities of $C_4H_{10}^+$ and $C_7H_{10}^+$, respectively, in order to make obvious the changing intensities of the peaks with respect to the hydrocarbon fragments as the deposition progresses. No $M_XO_Y^{\pm}$ ions were observed (data not shown). Based on our previous work with -CO_2H [27], -OCH_3 [28] and -CO_2CH_3 [26], the appearance of $MOCH_3^+$ ions but not $M_XO_Y^{\pm}$ ions indicates that the deposited metal has not undergone a redox interaction with

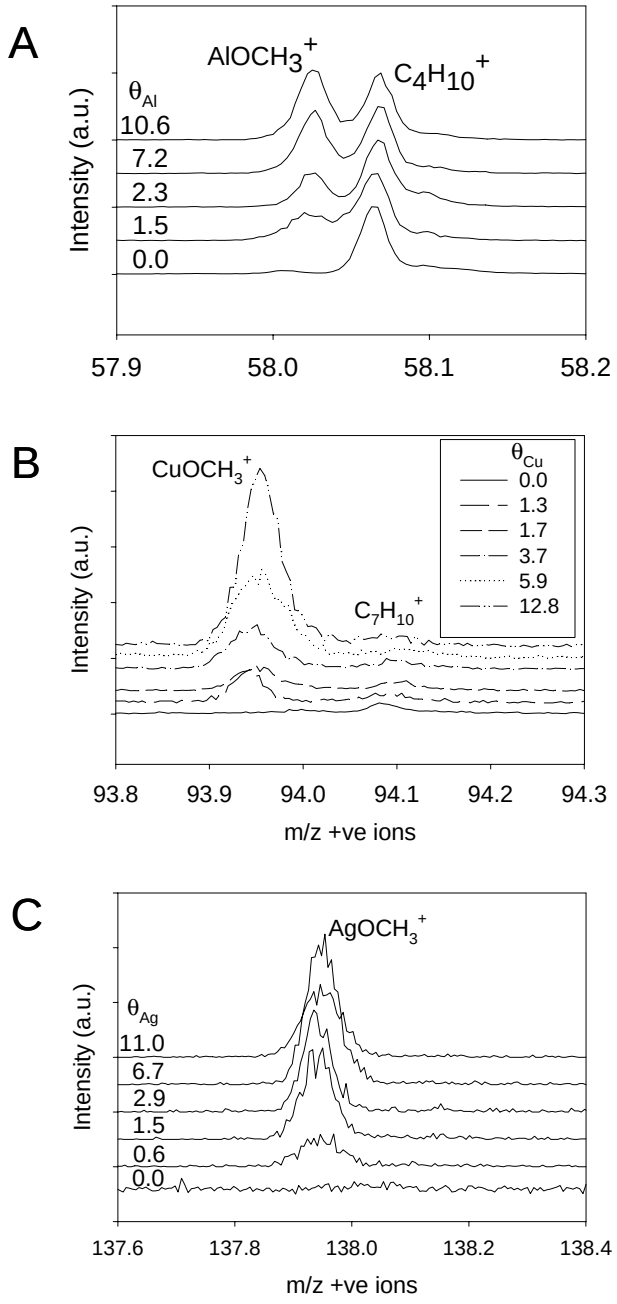

Figure 1: High resolution SIMS spectral overlays of $MOCH_3^+$ fragments. A, B and C represent positive ions of nominal mass 58 amu, 94 amu and 138 amu. The intensities in plots A and B are normalized to the initial peak intensity of $C_4H_{10}^+$ and $C_7H_{10}^+$, respectively.

the methoxy functionality to form M-O bonds, but signifies that the deposited metal atoms have only weakly interacted with the terminal group and stabilized at the SAM interface.

The metal atoms cannot exclusively be stabilized at the SAM surface since the data also show evidence for the penetration of the Al, Cu or Ag atoms to the S/Au interface [26,28], as shown by the appearance of MSH_2^+ (m/z = 61, 97, 141 respectively) peaks (Figure 2) and $Au_XM_YS_Z^-$ cluster ions (data not shown) for increasing increments of Al, Cu and Ag deposition. In Figure 2, the intensities of the MSH_2^+ (m/z = 61, 97, 141 respectively) peaks are shown for increasing increments of Al, Cu and Ag deposition. The $AlSH_2^+$, $CuSH_2^+$ and $AgSH_2^+$ spectra are normalized, respectively, to the initial peak intensities of $C_2H_5S^+$, $C_7H_{13}^+$ and $C_{10}H_{21}^+$ in order to make obvious the changing intensities of the peaks with respect to the hydrocarbon and substrate fragments as the deposition progresses. The increase of the relative MSH_2^+ and $Au_XM_YS_Z^-$ intensities throughout the low coverage deposition regime indicates the deposited metal atoms continuously penetrate at all coverages to the Au/S interface. Note the important contrast to the case of Al metal deposition on a CH_3-terminated SAM where penetration is observed to cease after an ~1:1 Al:Au adlayer forms [26].

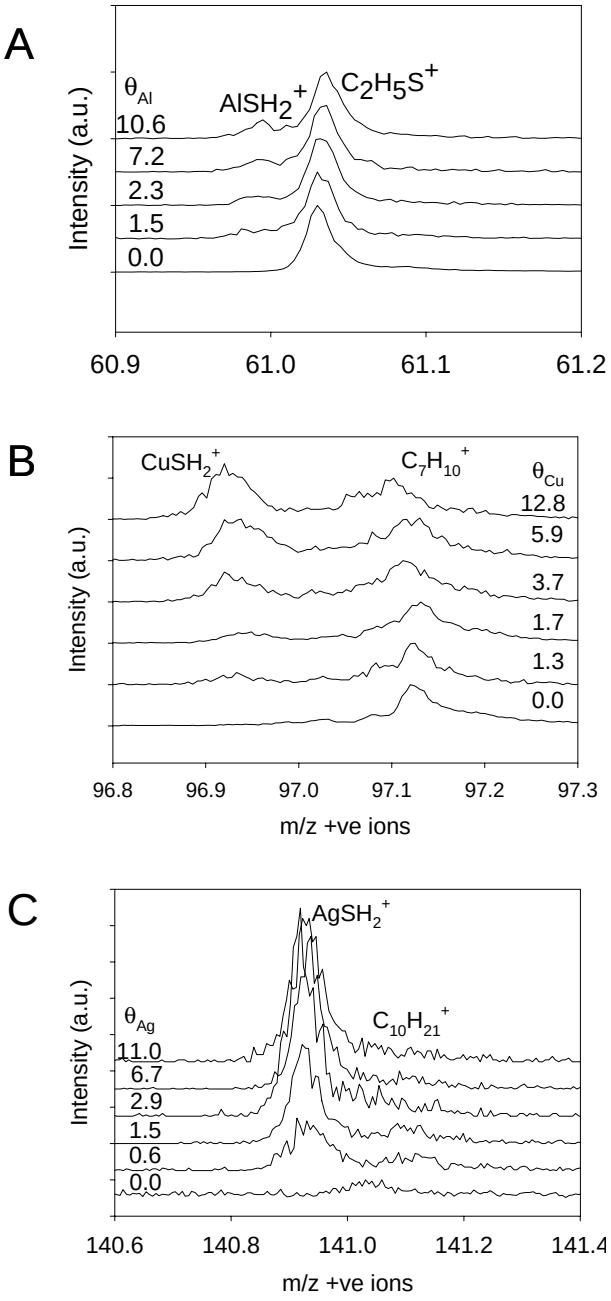

Figure 2: High resolution SIMS spectral overlays of MSH_2^+ fragments. A, B and C represent positive ions of nominal mass 61 amu, 97 amu, 141 amu. The intensities in plots A, B and C are normalized to the initial peak intensity of $C_2H_5S^+$, $C_7H_{13}^+$ and $C_{10}H_{21}^+$, respectively.

The state of the penetrated metal atoms is revealed by the observation that the monomer (M^+), dimer (M_2^+) and trimer (M_3^+) peak intensities (where M = Al, Cu, Ag), shown in Figure 3, increase proportionately with the first increment of deposited metal increase. Earlier we demonstrated that these signals differ between systems where deposited Al chemisorbs at the monolayer terminus and those where it penetrates through the monolayer to the S/Au interface [26-28]. When Al is first deposited onto a $–CH_3$ terminated SAM, which allows penetration, the Al^+ and Al_2^+ increase steadily whereas there is a slight delay in the Al_3^+ ion. In contrast, for the $–CO_2CH_3$ terminated SAM, when the first increments of Al are deposited on the monolayer (where Al chemisorbs) there is an increase in the Al^+ intensity, whilst there is a slight delay in the growth of the Al_2^+ and Al_3^+ ion intensities, which rise in tandem. Following this interpretation, the early growth of M_2^+ intensities support the conclusion that Al, Cu and Ag penetrate through the $–OCH_3$ terminated SAM to the Au/S interface.

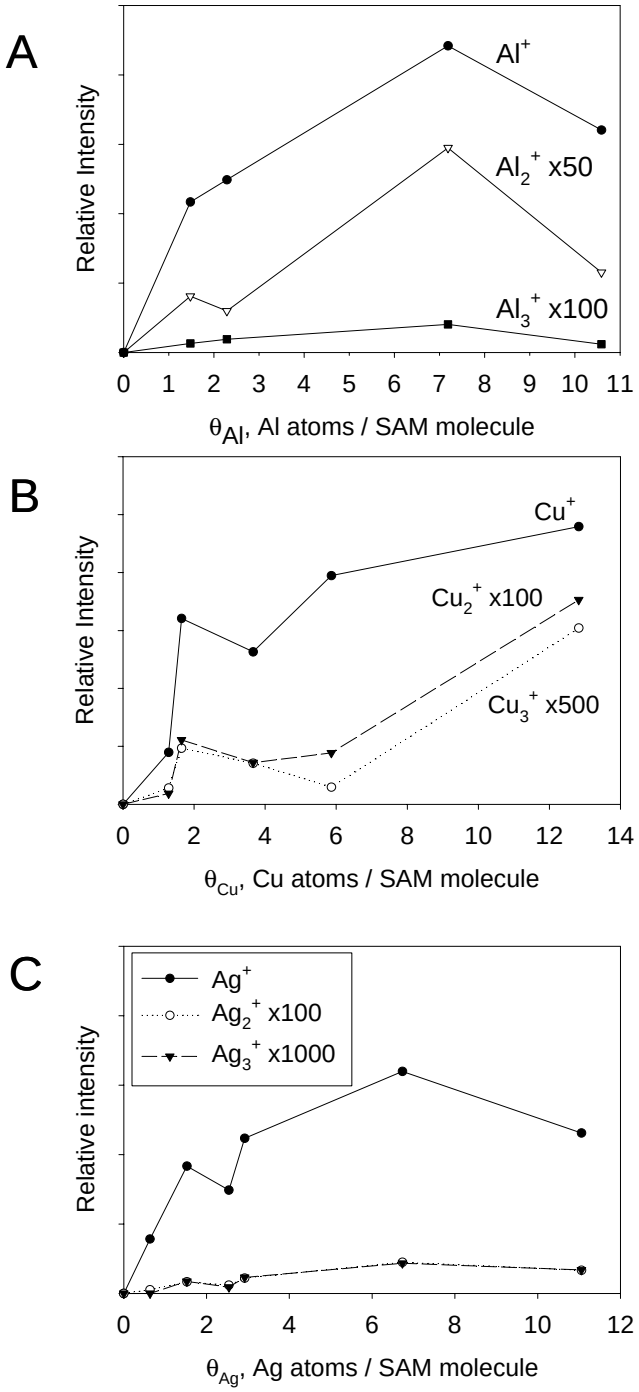

Figure 3: Integrated SIMS ion peak areas plotted versus θ_M for the OCH_3 SAM. A, B and C represent the peak areas of Al_n^+, Cu_n^+, and Ag_n^+, where n = 1–3, respectively.

After deposition of Al, Cu or Ag, another important diagnostic feature in the ToF-SIMS spectra is the relatively consistent intensity of the Au_2A^- and AuA_2^- peaks, which involve intact adsorbate molecules (A). Note in figure 4 how the areas of these peaks barely drop below their initial values at continued Al, Cu or Ag deposition (10.6, 27.0 and 16.2 ML respectively) indicating that the deposition of the metal leaves the adsorbate molecule chemically intact and thus, does not react with the $–OCH_3$ groups. In fact, the molecular ion peak intensities actually increase upon metal deposition, which is likely due to electron transfer, with increased ion yield, from the more electropositive deposited metal atoms to the more electronegative Au atoms and clusters leaving the surface [26]. Consistent with the lack of decrease of the molecular ion peak intensity, the hydrocarbon fragment peak intensities remain relatively unchanged during the early stages of the deposition (data not shown), as do the metal cluster peaks involving the Au substrate. As the deposition progresses, all peak intensities become increasingly attenuated, consistent with a growing metal overlayer that can block substrate ion ejection.

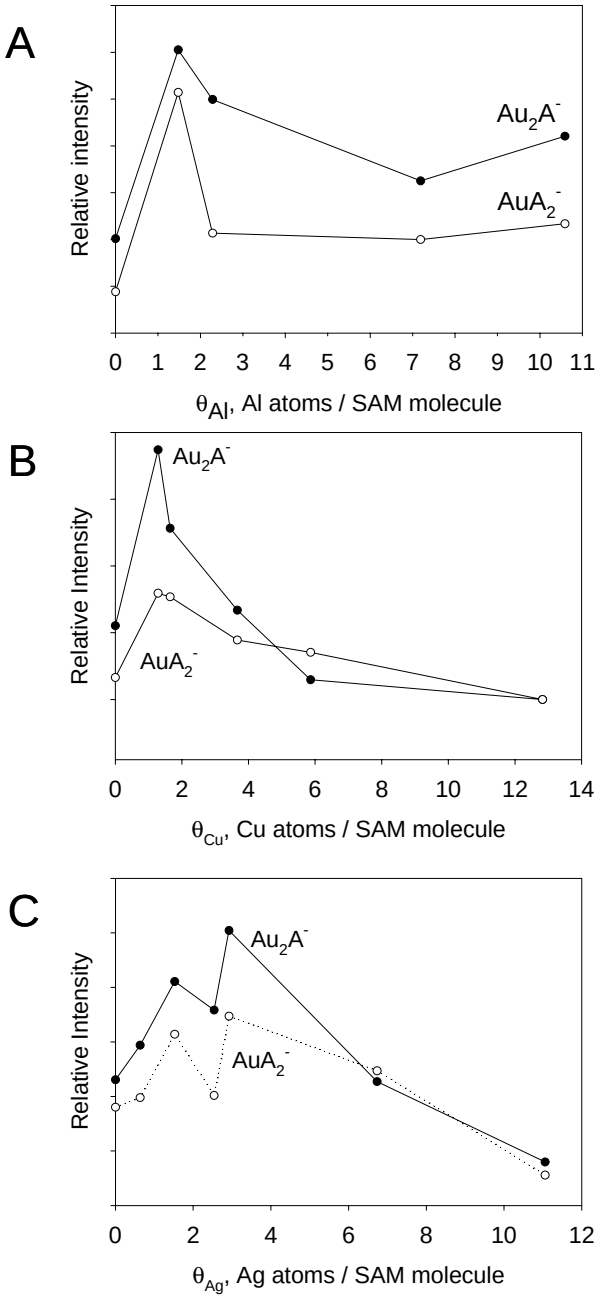

Figure 4: Integrated SIMS peak areas of Au_2A^- and AuA_2^- plotted versus θ_{Al} (A), θ_{Cu} (B) and θ_{Ag} (C).

3.1.2 Deposition of Au

In the positive ion mass spectrum, the absence $AuOCH_3^+$ and $AuO^{\pm}$ ions (data not shown) indicates that the Au atoms do not interact with the terminal $–OCH_3$ group. We do conclude, however, from the appearance of the $AuSH_2^+$ peak intensity, shown in figure 5a, that deposited Au atoms penetrate to the Au/S interface. Penetration through the SAM is supported by STM measurements of Ohgi *et al* [61] who reported that deposition of Au atoms on an octanethiolate ($CH_3(CH_2)_7S$-) on Au {111} forms islands at the Au/S interface. At $\theta_{Au} \sim 6–7$, these islands were observed to coalesce into a smooth surface. Such morphology changes lead to changes in the observed secondary ion mass spectra. The initial surface roughening will lead to the formation of Au moieties with a lower coordination, which should make the ejection and ionization of departing fragments and clusters easier. Once the surface smoothes upon continued Au deposition, the efficiency of the ejection / ionization of Au clusters and fragments is reduced. Indeed, the data, shown in figure 5a, do follow this trend of increasing then decreasing $AuSH_2^+$ peak intensities.

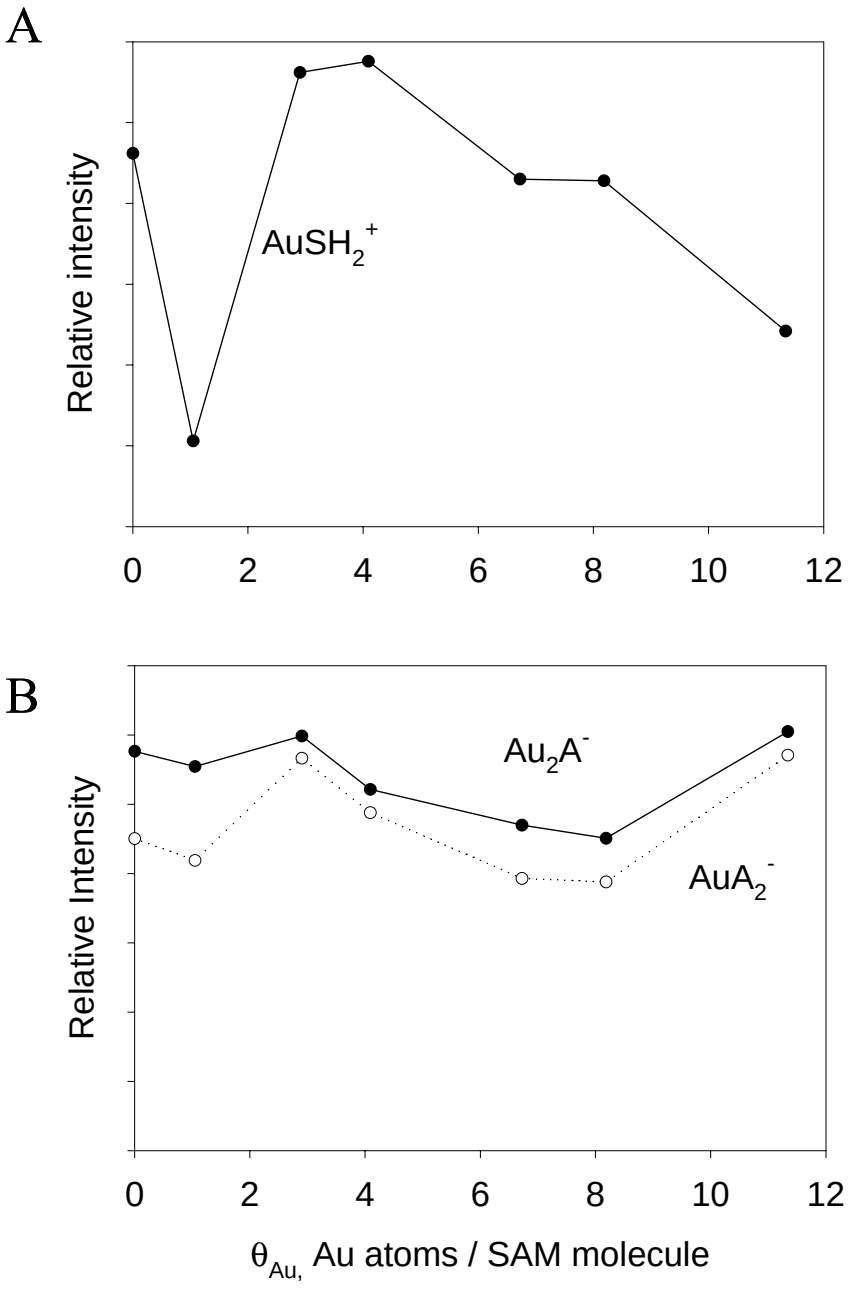

Figure 5: Integrated SIMS peak intensities of (a) $AuSH_2^+$ and (b) Au_2A^- and AuA_2^- plotted versus θ_{Au}.

Since a new Au adlayer is being formed, one would expect that the deposited Au atoms to continuously penetrate through the SAM layer to Au/S interface. The relatively constant intensities of the AuA_2^- and Au_2A^- ions, which involve intact adsorbate molecules, support this behavior (Figure 5b; the variation in the intensity is mainly dues to integration errors.). Even after a deposition of $\theta_{Au} \sim 124$, the Au_2A^- and AuA_2^- yields are ~ 70 % of those of the bare monolayer indicating that there is little, or no, Au overlayer formation even at this high coverage. Therefore, these data confirm that Au is penetrating through the monolayer throughout the deposition range with no metallic overlayer forming. Hence the $–OCH_3$ terminated SAM "floats" on top of the deposited Au interlayer.

3.2 IRS

The IR assignments for the bare monolayer have been reported previously [28,42]. Relevant peaks in the low and high frequency ranges, 750-1600 cm^{-1} and 2700-3100 cm^{-1} respectively, are summarized here for reference. The peaks at 1132, 1390 and 1465 cm^{-1} are assigned as the C-O-C antisymmetric stretch (ν_{C-O}), the $–CH_3$ symmetric deformation (δ_{CH_3}) and the $–CH_2–$ scissor deformation (δ_{CH_2}) respectively. In the high frequency regime, the $–CH_2–$ d^+ and d^- stretches are assigned at 2851 and 2918 cm^{-1}, and the peaks at 2811, 2828 and 2981 cm^{-1} are attributed to the various stretching modes of the terminal CH_3 group. The data indicates that the bare monolayer is well-organized with the chains primarily in an all trans conformation [39].

The IR spectra of the monolayer before and after metallization with Cu, Ag and Au at $\theta_M = 100$ (M = Cu, Ag, Au), and Al at $\theta_{Al} = 50$ are shown in Figure 6. In each case, we observe the preferential attenuation of the modes associated with the $–OCH_3$ group. The observed attenuation is more pronounced upon deposition of Al than upon Cu, Ag and Au

deposition. At θ_{Al} = 50, the intensity of ν_{C-O} (1132 cm^{-1}) has been reduced by ~80 % of its original value, the intensity of δ_{CH_3} (1390 cm^{-1}) has disappeared into the baseline noise and there is a significant loss of intensity of modes associated with the CH_3 group (2811, 2828 and 2981 cm^{-1}). In contrast, the intensities of the $–CH_2$- bend and stretch modes at 1465, 2851 and 2918 cm^{-1} show slight attenuation but indicate the monolayer chains are still well-ordered. Upon deposition of 100 ML of Cu, Ag and Au, the intensity of ν_{C-O} mode is reduced by ~75 %, ~50 % and ~50 % respectively of its original value. It is also observed that the intensity of δ_{CH_3} has disappeared into the baseline noise and there is a slight attenuation of the CH_3 modes. The intensities of the $–CH_2–$ bend and stretch modes are also slightly attenuated but, as with deposition of Al, indicate the chains remain well ordered. We also note that upon deposition of Cu, Ag, and Au a shoulder on the low frequency side of the $–CH_2–$ d^- mode (~2906 cm^{-1}) also grows in. As well as this feature, upon deposition of Cu and Ag a second small feature grows in at 1022 cm^{-1}. An experiment using $HS-(CH_2)_{16}-OCD_3$ monolayers indicates that the feature at 2906 cm^{-1} is due to the methylene backbone of the SAM, and not the terminal methoxy group. To date, we however have not been able to exclusively assign these modes.

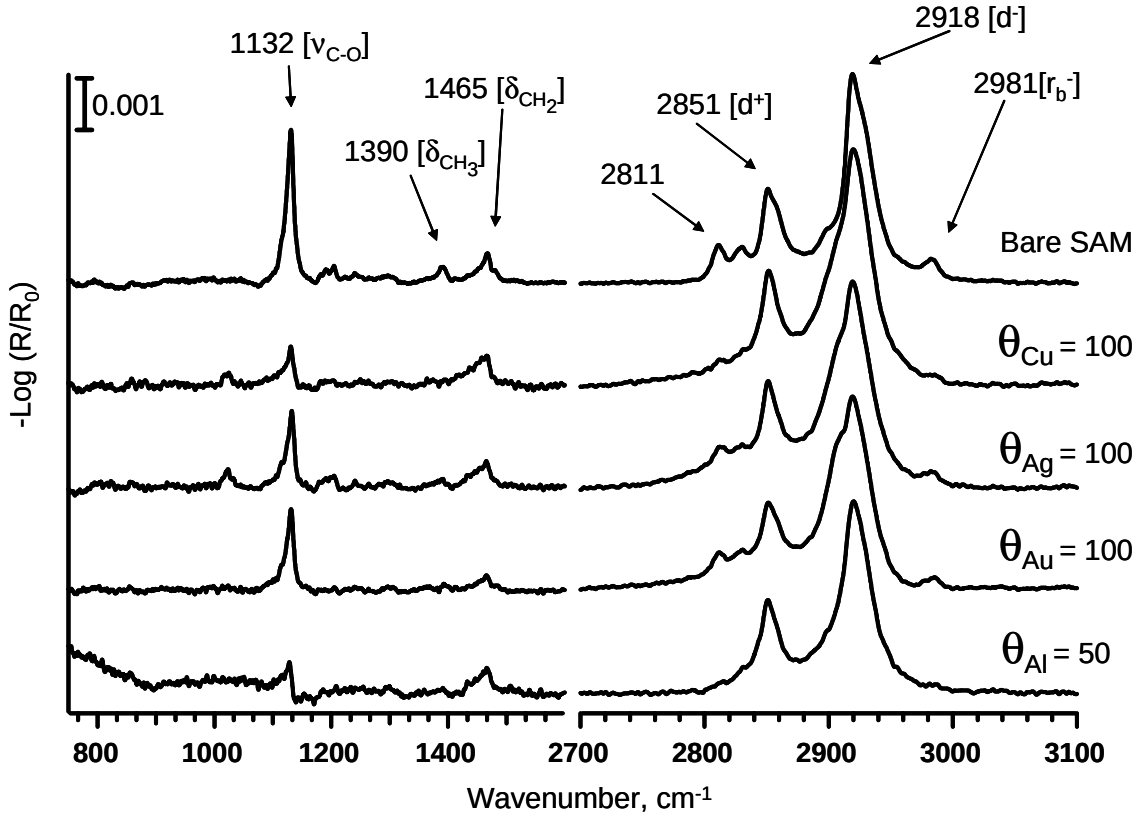

Figure 6: Low and high frequency region IRS spectra of the bare OCH_3 SAM and upon Al, Cu, Ag and Au deposition.

The attenuation of IR modes can be caused by chemical reactions, reorientation of the monolayer dipoles with respect to the surface [39], or by screening of the dipole due to metal atoms, clusters or overlayers [2]. Since we do not observe the appearance of new absorption bands, such as the Al-O stretch (855 cm^{-1}) [26-28], and given the ToF SIMS results we conclude that there is no significant chemical interaction between the deposited metal atoms and the methoxy-terminated SAM. We therefore attribute the observed attenuation to the reorientation of the monolayer dipoles, screening of the surface dipoles, or a combination of these effects.

4. Discussion

All the present data for Cu, Ag and Au, and the previous data for Al [26-28,36] are consistent with a general mechanism in which the deposited metal atoms can: a) interact with the terminal group and stabilize at the SAM surface [28,36]; and/or b) penetrate through the film [21,26,28]. In addition, for more reactive metals one can include these mechanisms: c) react with the terminal group whilst preserving the SAM methylene backbone [19,26,27]; d) react with and destroy the monolayer, an obviously undesirable result [19,62]; or e) a combination of these mechanisms [28,36]. These reaction pathways can be summarized as follows:

Condensation	$M_g \leftrightarrow M_S$	(1)
Complexation	$SAM + M_S \leftrightarrow SAM \cdots M$	(2)
Bond Insertion (Organometallic formation)	$SAM + M_S \rightarrow SAM - M$	(3)
Penetration	$AuS(CH_2)_{16}OCH_3 + M_S \rightarrow AuMS(CH_2)_{16}OCH_3$	(4)

where M_g and M_s represents the deposited metal atoms in the vapor and surface adsorbed states respectively and SAM denotes the alkanethiolate adsorbed on the Au surface, $AuS(CH_2)_{16}OCH_3$. While the adsorption mechanism (1) is considered to be reversible, our

results, in particular ToF SIMS data, indicate that the metal atoms do not desorb from the SAM surface during the experiment [63]. The equilibrium in step (2) implies that the surface adsorbed metal atoms can rapidly diffuse between preferred sites at the SAM/vacuum interface.

The experimental data indicate that the deposited Al, Cu, Ag and Au atoms do not insert into the $–OCH_3$ group to form a M-O bond and therefore reaction pathway (3) is not operative [see section 4.1 below]. The experimental data indicate that the deposited Al, Cu and Ag metal atoms penetrate to the Au/S interface and also interact with the methoxy terminal group. Thus reaction pathways 1, 2 and 4 are operative. For Au metal deposition, the metal atoms only penetrate to the Au/S interface and hence mechanisms 1 and 4 are operative.

The discussion will proceed by first examining the interaction of the deposited Cu and Ag atoms with the $–OCH_3$ group and then comparing the results to the case of Al atoms [28]. This will be followed by the elucidation of the metal atom penetration mechanism to the Au/S interface. A schematic diagram of the overall deposition processes, deduced from the experimental data, is shown in figure 7.

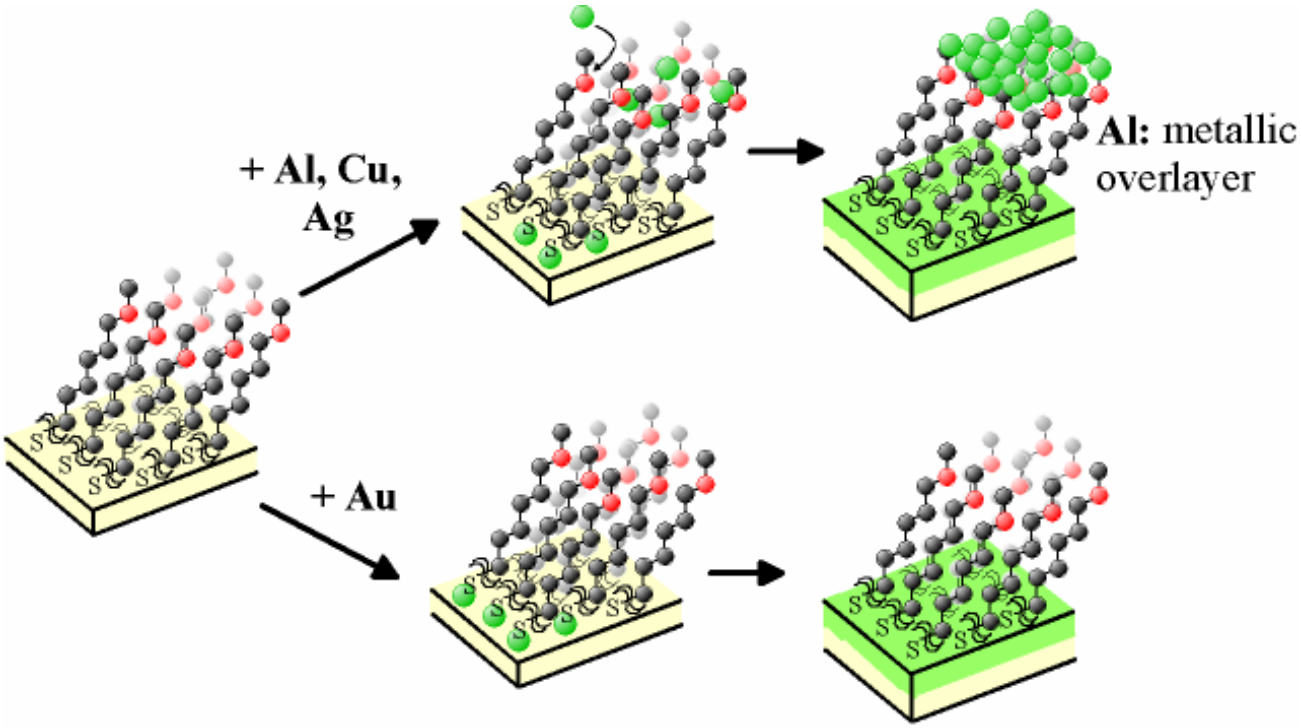

Figure 7: Schematic illustrations of the important features of the reaction pathways including the steric hindrance of the metal – oxygen interaction. Metal atom is represented in green, oxygen in red and hydrocarbons in black.

4.1 Interaction of Deposited Metal Atoms with the –OCH_3 Group

Following condensation of the metal atoms on the SAM surface (step 1) the evolution of the metal–SAM interaction is governed by the interplay of the localization of the metal atoms at the –OCH_3 groups (step 2), followed by overlayer film nucleation and growth, and penetration to the Au/S interface (step 4). Note that for Au atom deposition only penetration to the Au/S interface is observed (step 4). The presence of $MOCH_3^+$ ions, where M = Al, Cu, Ag, and not $M_XO_Y^{\pm}$ ions in the ToF SIMS spectra (figure 1) demonstrates a M···OCH_3 association, consistent with the presence of a stabilizing interaction between the Al, Cu and Ag atoms and the –OCH_3 group. Further evidence that the deposited metal atoms do not insert into the terminal group is the nearly constant character (i.e. the peak shape and position) of the C-O stretch mode at 1132 cm^{-1} (Figure 6). We note that this interaction is sufficiently strong to localize metal atoms on the surface such that subsequent nucleation and growth of a metal overlayer may occur, but sufficiently weak so that penetration of the metal atoms remains competitive.

In the case of Cu and Ag, the localization and penetration of metal atoms appear to be balanced such that both processes occur continuously (see section 4.2 below). In the case of Al atoms, both localization at the vacuum interface and penetration occurs initially, but at higher metal coverages the metal atom penetration ceases and a metallic overlayer forms [28,36]. Further the detailed electronic and steric nature of the M···OCH_3 interaction is quite subtle as evidenced by the Al···OCH_3 interaction. Upon Al deposition, the C-O stretching mode, a general measure of the bond strength, is barely perturbed at low coverages (figure 6) while the –**C**H_2O**C**H_3 C1s XPS binding energy, a measure of local electron density, shifts to lower values and is hidden by the main C1s peak [28,36].

In order to better understand this metal – terminal group interaction, quantum mechanical calculations were applied to the isolated model systems M + CH_3OCH_3 and $CH_3CH_2CH_3$, where M = Al, Cu, Ag and Au, to investigate the energetics of the stabilization process (table 1). Previous calculations on the Al $–OCH_3$ interaction at the B3PW91/6-311+G(2df,p) level of theory [28] demonstrated that the lowest energy configuration, -272 kJ mol^{-1}, involves the *insertion* of Al into the C-O bond, with a lesser minimum of -89 kJ mol^{-1} for C-C bond insertion. Since neither of these processes is observed experimentally, it was assumed that the activation barriers for these processes are prohibitively high [28]. In the present calculations for insertion of Cu, Ag and Au into the C-O bond, the calculations failed to converge implying that these complexes are unstable. Furthermore, calculations of the insertions of Cu, Ag and Au into the C-C bond showed that the products were unstable by 48, 142 and 52 kJ mol^{-1} respectively and thus would not be observed, in agreement with experimental data.

Table 1: DFT Calculated Stabilization Energies for Various Metal-Oxygen Complexes

Molecule	Complex	Metal	Stabilization Energy (kJ/mol)	
			LANL2DZ	6-311+G(2df,p)
	O···Al	Al	-52	-33
CH_3-O-Al-CH_3	O-Al-C	Al	-261	-272
C_2H_5-Al-CH_3	C-Al-C	Al	-69	-90
	O···Cu	Cu	-34	
CH_3-O-Cu-CH_3	O-Cu-C	Cu	Failed	
C_2H_5-Cu-CH_3	C-Cu-C	Cu	48	
	O···Ag	Ag	-13	
CH_3-O-Ag-CH_3	O-Ag-C	Ag	Failed	
C_2H_5-Ag-CH_3	C-Ag-C	Ag	142	
	O···Au	Au	-17	
CH_3-O-Au-CH_3	O-Au-C	Au	Failed	
C_2H_5-Au-CH_3	C-Au-C	Au	52	

For these systems, however, secondary minima at –52, -34, -13 and –17 kJ mol^{-1} are found involving complexation type of interaction between Al, Cu, Ag and Au and the O atom of the $–OCH_3$, respectively (table 1). Note that while Au shows greater stabilization by the $–OCH_3$ group than Ag, Au exclusively penetrates to the Au/S interface. One explanation for this apparent contradiction is that the activation barrier for Au localization at the $–OCH_3$ group is prohibitively high relative to the Ag case. Experimental data indicate that Au is not stabilized at the SAM/vacuum interface and thus we assume that the activation barrier for this interaction is prohibitively high.

For Al, Cu and Ag, the minimum energy geometries for the $M\cdots O(CH_3)R$ interaction places the metal atom near the O atom, away from the C-O-C bonds. Geometric considerations indicate that this optimum isolated cluster geometry will be unfavorable in the SAM case due to the steric hindrances at the SAM/vacuum interface (Figure 7). While a small number of $–OCH_3$ groups may be able to undergo conformational re-configuration to allow optimal metal atom-methoxy group interactions; however, most terminal groups will not be able to re-orient due to molecular packing in the SAM. Thus we expect that the average stabilization energy per deposited metal atom will be considerably reduced relative to the isolated system. This picture is consistent with the minor perturbations observed in the IR C-O stretching frequencies (figure 6). Given the low rotational barrier of the $RC(H_2)$-OCH_3 bond relative to the C-C bonds [28], a wide range of $M\cdots OCH_3$ geometries are possible within the constraints of the intrinsic chain terminus geometry (figure 7). Thus the metal-surface interaction can be considered as a quasi-isotropic weak solvation of the metal by the $–OCH_3$ terminal group, as suggested previously for the case of Al [64].

4.2 Penetration Mechanism to the Au/S Interface

The experimental data indicate that the deposited metal atoms penetrate to the Au/S interface since in the ToF SIMS spectra, we observe peaks of the form MSH_2^+ where M = Al, Cu, Ag or Au. In this discussion it is useful to refer to the schematic in Figure 8 which summarizes important aspects of the metal penetration process.

First we shall review the previously reported cases of Al deposition on $–OCH_3$ [28] and $–CH_3$ terminated SAMs [22]. It was concluded, primarily from the ToF SIMS data, that for the $–CH_3$ terminated SAM, penetration of Al atoms ceases to increase at $\theta_{Al} \sim 2.7$, at which point the data indicated the onset of Al overlayer growth at the SAM/vacuum interface. In contrast, for the $–OCH_3$ SAM case, penetration continues even at $\theta_{Al} \sim 12.2$. This behavior was explained on the basis that the penetration of Al atoms to the Au/S interface continues until an ~1:1 Al:Au adlayer is formed, after which the penetration path closes and further deposited metal atoms form an overlayer at the SAM/vacuum interface. It is reasonable to presume that the penetration path closes for the $–OCH_3$ case if sufficient Al were deposited to produce an ~1:1 Al:Au interfacial layer because the $–CH_3$ and $–OCH_3$ groups should have a negligible effect on the characteristics of the S/Au interface, located 16 C atoms from the chain terminus. The penetration mechanism was proposed to occur via the thermally driven translational motion (hopping) of the adsorbate molecules on the Au substrate lattice, which leads to the transient appearance of holes (defects) between the chains sufficiently large to provide channels for metal atom diffusion to the S/Au interface (see the upper part of Figure 8).

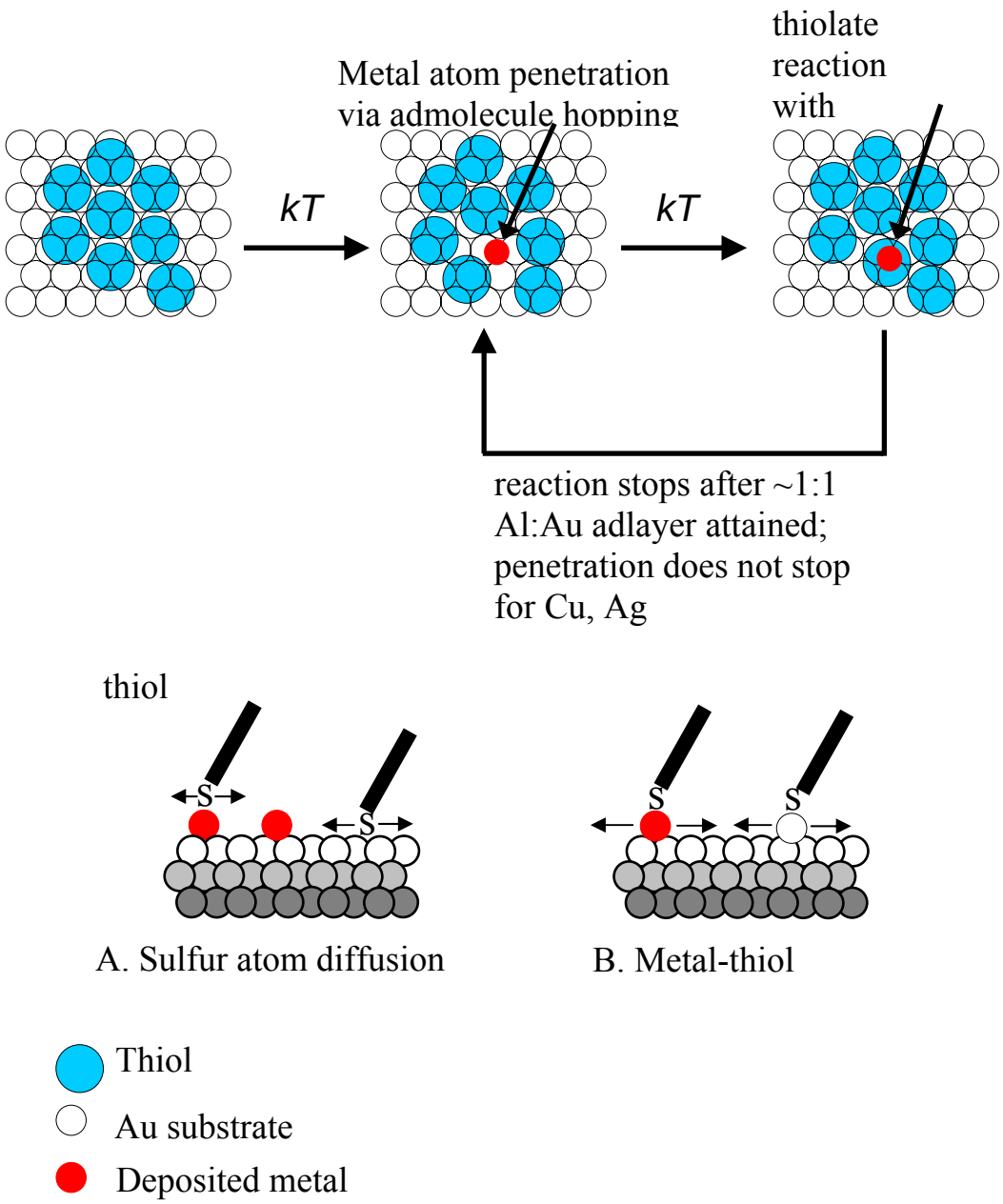

Figure 8: Cartoon illustrations of thiol (sulphur atom) or M-Th, where M = metal atom and Th = thiol, diffusion across the Au surface.

One test of this hopping hypothesis is to examine the Al/-OCH_3 interaction at high Al depositions, where one might expect that the ~1:1 Al:Au adlayer would have formed closing the penetration pathway. At a coverage of θ_{Al} ~192, the ToF SIMS data indicate that a metallic Al overlayer has formed and that the –OCH_3 SAM has been completely covered by the deposited Al; no fragment or cluster ions associated with the methoxy–terminated SAM are observed. Further, previous XPS data [28] also indicate that Al ceases to penetrate to the Au/S interface at lower coverages while further increments of deposited Al atoms form a metallic overlayer.

In contrast, Cu, Ag and Au atoms continue to penetrate to the Au/S interface at very high metal coverages. After deposition of θ_{Cu}~176, θ_{Ag}~130 and θ_{Au}~124, we observe significant peak intensities of both cluster and fragment ions associated with the –OCH_3 SAM layer in the ToF SIMS spectra. For example, at θ_{Cu}~176 the intensities of $CuSH_2^+$ (penetration) and $CuOCH_3^+$ (Cu-OCH_3 interaction) are ~80 % of the observed maximum peak intensity, and at θ_{Ag}~130 the intensities of $AgSH_2^+$ and $AgOCH_3^+$ are ~85–90 % of the observed maximum peak intensity. These data are consistent with the XPS results. For example, in the case of Ag deposition (Figure 9), we observe that with increasing Ag coverage the Au 4f signal intensity is significantly attenuated; at θ_{Ag}~37, only ~1% of the original Au 4f signal intensity remains, whereas the intensities of the C 1s and O 1s peaks remain relatively constant. Thus the SAM remains close to the vacuum interface while the

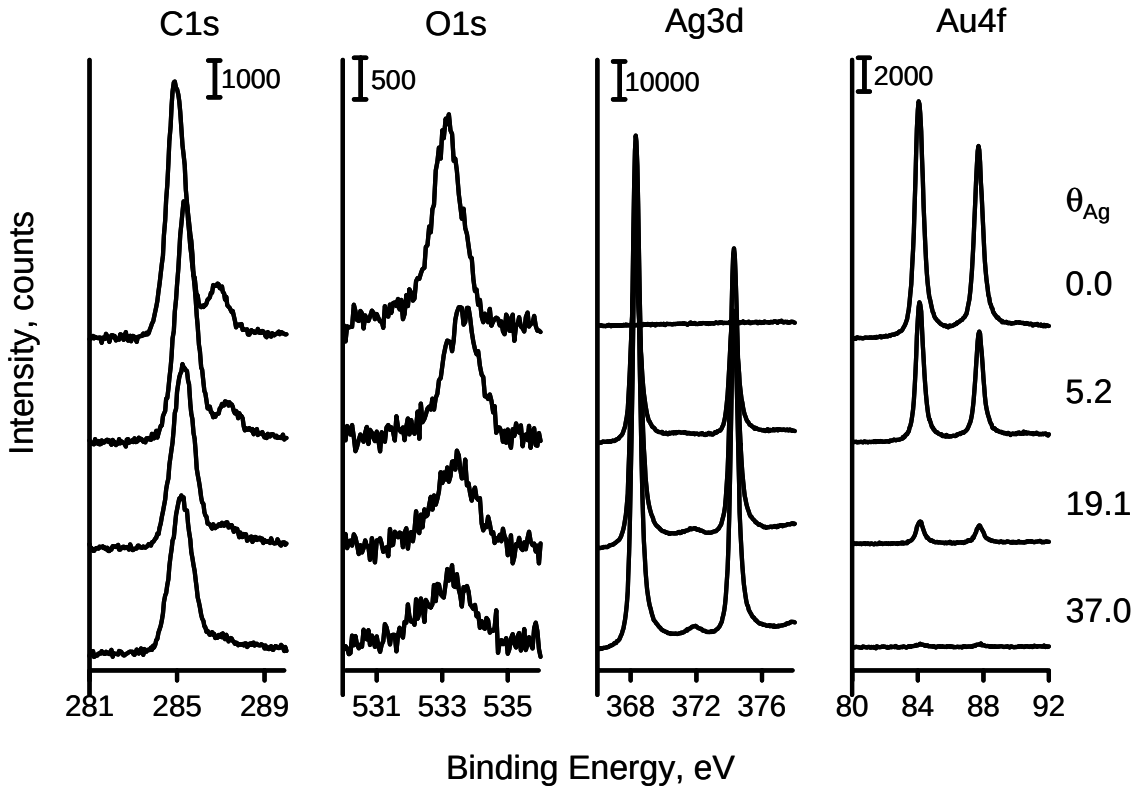

Figure 9: The core level XPS spectra of the $–OCH_3$ SAM prior to and following deposition of Ag. A, B, C and D represent the C1s, O1s, Ag3d and Au4f respectively.

Au has been completely buried by the deposited Ag layer. This indicates that Ag atoms continue to penetrate through the SAM layer at all coverages.

A satisfactory model for the penetration pathway must be able to explain why: a) the Al penetration channel is closed after ~1:1 Al:Au adlayer has formed; but b) the penetration of Cu, Ag and Au continues even at very high metal coverages. Our previously proposed penetration mechanism involved the diffusion of metal adatoms from the vacuum surface to lower energy positions at the Au/S interface [22,28,65]. In the case of Al, as the Al atoms accumulate at the Au/S interface and they were proposed to insert into the Au-SR bonds (R = alkyl) to form Al-SR bonds as indicated by the formation of $Au_XAl_YS_Z^-$ ions. If the formation of these bonds slows or stops the formation of transient defects, this would explain the closure of the penetration channel upon completion of ~1:1 Al:Au adlayer. A schematic figure of this process is shown in figure 8.

If this reaction pathway is correct, the different observed behaviors for Al, Cu, Ag and Au must correlate with the energetics of the diffusing species. Specifically, the central issue is whether the lowest energy pathway for the lateral motion of the SAM moiety is motion of a metal-alkanethiolate (-MSR) across the Au substrate surface (or metal adlayer at high coverages) or motion of an alkanethiolate moiety (-SR) across the metal adlayer (M) surface. In order to examine these possibilities one needs to estimate the activation barriers for lateral hopping (diffusion) of these species. An easy way to do this is to assume that these activation barriers correlate with the trends in the different bond energies involved, either M-SR or Au-MSR (M-MSR at higher coverages).

There is some evidence from the literature that suggests that the correct mechanism does not involve M-SR bonds, ie. alkanethiolate hopping. Using ultraviolet photoelectron

spectroscopy, XPS and work function measurements Shen and Nyberg suggested that the Al-SR bond is weaker than the Cu-SR bond [66]. Since the penetration of Cu continues well past the formation of an ~1:1 M:Au adlayer in contrast to the case of Al where penetration ceases, it is apparent that formation of Cu-SR bonds is much less efficient at closing the penetration channel. This would rule out the alkanethiolate (-SR) chain hopping model.

To investigate in more detail the energetics of the alkanethiolate (-S atom) hopping model, quantum mechanical calculations were applied to the isolated model system $M\text{-}S(CH_2)_5OCH_3$ where M = Al, Cu, Ag, Au. The results are summarized in table 2. If the $E_{M\text{-}S} > E_{Au\text{-}S}$ bond, where E = bond dissociation energy, one would predict that the metal atom would insert into the Au-S bond to form a Au-M-SR structure and that the penetration of the deposited metal atoms will cease after ~1:1 metal:Au adlayer has been attained. For Ag, $E_{Ag\text{-}SR}$ = 173 kJ mol^{-1} is close to $E_{Au\text{-}SR}$ = 179 kJ mol^{-1} and thus, in agreement with experiment, one would expect that the penetration pathway would not close since the barrier for the lateral diffusion of -SR species will remain approximately the same before and after deposition. For Al and Cu, $E_{Al\text{-}SR}$ and $E_{Cu\text{-}SR}$ = 292 and 227 $kJmol^{-1}$ respectively, are larger than $E_{Au\text{-}SR}$ = 179 $kJmol^{-1}$. Hence, in agreement with the observed experimental data both Cu and Al will insert into the Au-SR bond. However, if –SR diffusion across the surface were occurring then given the bond energies and the experimental results for Al deposition [28], one would also predict that penetration of deposited Cu atoms would cease after an ~1:1 adlayer has been attained, in conflict with the observed continuous penetration of Cu atoms. This conclusion points to the metal-alkanethiolate (-MRS) diffusion as the critical step for closure of the penetration pathway (Figure 7). Support for

this mode of surface diffusion is given by results of previous STM studies in which gold-alkanethiolate moieties (Au-SR) have been observed to diffuse across a Au {111} surface [67,68].

Table 2: DFT Calculated Bond Energies for various Metal-Thiol Complexes

Complex	Metal	Binding Energy (kJ/mol)	S-M1 Distance (Å)	M1-M2 Distance (Å)
$CH_3O(CH_2)_5$**S–Au**	Au	179	2.36	
$CH_3O(CH_2)_5$**S–Al**	Al	293	2.36	
$CH_3O(CH_2)_5$**S–Ag**	Ag	174	2.42	
$CH_3O(CH_2)_5$**S–Cu**	Cu	228	2.2	
$CH_3O(CH_2)_5$S**Au-Au**	Au	118	2.4	Au-Au= 2.56
$CH_3O(CH_2)_5$S**Au-Al**	Al	200	2.45	Au-Al= 2.46
$CH_3O(CH_2)_5$S**Al-Au**	Au	164	2.29	Al-Au= 2.43
$CH_3O(CH_2)_5$S**Al-Al**	Al	78	2.31	Al-Al= 2.78
$CH_3O(CH_2)_5$S**Au-Ag**	Ag	97	2.42	Au-Ag= 2.64
$CH_3O(CH_2)_5$S**Ag-Au**	Au	95	2.48	Ag-Au= 2.62
$CH_3O(CH_2)_5$S**Ag-Ag***	Ag	83	2.63, 2.65	
$CH_3O(CH_2)_5$S**Au-Cu**	Cu	128		
$CH_3O(CH_2)_5$S**Cu-Au**	Au	124	2.23	Cu-Au= 2.42
$CH_3O(CH_2)_5$S**Cu-Cu***	Cu	123	2.38, 2.39	

*Most of the metal dimer complexes form a chain structure: S-M1-M2. These two structures, however, have both metals complexed directly to the sulfur atom.

Quantum mechanical energy calculations for the isolated model system M + $AuS(CH_2)_5OCH_3$ (AuSR), where M = Al, Cu, Ag and Au, are summarized in table 2 and support the metal-alkanethiolate diffusion mechanism. First we note that $E_{Au\text{-}SR}$ (= 179 kJ mol^{-1}) > $E_{Au\text{-}AuSR}$ (= 118 kJ mol^{-1}) which suggests that there is a lower energy barrier for diffusion of –AuSR than for –SR across the Au surface, in agreement with the STM data [67,68]. For Al, Cu and Ag, $E_{M\text{-}SR}$ = 293, 228 and 174 kJ mol^{-1} respectively, is larger than the gold-metal alkanethiolate bond energy, $E_{Au\text{-}MSR}$ = 164, 124 and 95 kJ mol^{-1} repectively, suggesting that the –MSR species controls surface diffusion across the Au substrate.

The remaining question of whether the penetration channel closes can be readily explained on the basis of the Au-MSR energies. First, since $E_{Au\text{-}AlSR}$ (= 164 kJ mol^{-1}) > $E_{Au\text{-}AuSR}$ (= 118 kJ mol^{-1}) one would expect that the rate of the diffusion of the alkanethiolate chains would rapidly decrease once the –AlSR species has formed at the Au/S interface and thus penetration of deposited Al atoms will cease after an ~1:1 Al:Au adlayer has been attained. Second, since $E_{Al\text{-}AlSR}$ (= 78 kJ mol^{-1}) < $E_{Au\text{-}AlSR}$ (= 164 kJ mol^{-1}) it is energetically unfavorable for a second adlayer of aluminum to be deposited, in agreement with our experimental data. Finally, we also note that $E_{Al\text{-}AuSR}$ (= 200 $kJmol^{-1}$) > $E_{Au\text{-}AlSR}$ (= 164 kJ mol^{-1}). However, it is unlikely that there would be an exchange in the Au and Al atoms at the interface since this interaction is endothermic [69].

$$Au\text{-}Al\text{-}S(CH_2)_5OCH_3 \rightarrow Al\text{-}Au\text{-}S(CH_2)_5OCH_3 \qquad \Delta E = 78 \text{ kJ mol}^{-1}$$

For Cu and Ag, $E_{Au\text{-}MSR}$, = 124 and 95 kJ mol^{-1} respectively, is similar to that for Au $E_{Au\text{-}AuSR}$ = 118 kJ mol^{-1}. Hence one would not expect the rate of the diffusion of the alkanethiolate chains to vary much between the Au, Au-Cu and Au-Ag interfaces and thus the metal penetration pathway would not close, as observed in our experiments. We also

note that $E_{M\text{-}MSR}$, where M = Cu, Ag, is approximately $E_{Au\text{-}MSR}$ so there is no energy barrier to the continued deposition of metal atoms at the sulphur/substrate interface.

5. Conclusions

Upon vapor deposition of aluminum, copper and silver onto a $–OCH_3$ terminated hexadecanethiolate on Au {111}, the metal atoms simultaneously penetrate to the Au/S interface, where a stable adlayer forms, and stabilize at the $–OCH_3$ SAM surface. In the case of Al, the penetration channel closes after ~1:1 Al:Au adlayer has been attained, similar in overall character to the previously studied case of a $– CH_3$ terminated SAM [26]. In contrast for Cu and Ag deposition, the penetration channel does not close. To explain these observations, we propose that the penetration occurs via transient defects that arise from thermally activated diffusion of metal-alkanethiolate moieties, -MSR where M = Au, Al, Cu and Ag and R = $(CH_2)_{16}OCH_3$. As the deposition progresses, deposited metal atoms accumulate at the Au/S interface and insert into the Au-SR bonds to form M-SR bonds. Upon deposition of Al, the Au-AlSR bond is stronger than the Au-AuSR bond and thus has a higher energy barrier to diffusion, eliminating or greatly reducing the formation of transient defects. Upon completion of ~1:1 Al:Au adlayer, the penetration channel closes and further deposited Al atoms form an overlayer at the SAM/vacuum interface. In contrast, the Au-AgSR and Au-CuSR bond strengths are weaker or about the same strength as the Au-AuSR bond. Thus, these moieties are able to diffuse across the surface leading to the formation of transient defects, and hence penetration to the S/substrate interface continues at all metal coverages.

Finally, gold, an almost inert metal, does not interact with the methoxy terminal group. Rather, penetration of deposited Au atoms to the Au/S interface is observed at all coverages studied which leads to the interesting result of a "floating" SAM.

Experiments are underway to further examine the crucial details of these metal deposition mechanisms including *in-situ* atomic force microscopy to characterize the lateral distribution of the overlayer metal, cooling experiments to characterize the temperature dependent behavior of the competition between penetration and overlayer formation, and varying the alkanethiolate chain length from even to odd numbers of CH_2 groups to alter the steric environment of the terminal $-OCH_3$ group.

This study, in conjunction with previous studies [26-28], provides a basis for the rational design and control of many types of metallized organic structures ranging from metallized polymer surfaces, with strong metal adhesion and controlled morphology, to highly optimized electrical contacts in organic and molecular electronic devices.

6. Acknowledgements

The authors acknowledge financial support from the Office of Naval Research and National Science Foundation. A.V.W. would also like to thank Lev Gelb for many useful discussions.

7. References

1. Pireaux, J.J.; *Syn. Met.*, **1994**, *67*, 39-46

2. Strunksus, T.; Grunze, M.; Kochendoerfer, G.; Wöll, Ch.; *Langmuir*, **1996**, *12*, 2712-2725

3. Faupel, F.; Willecke, R.; Thran, A.; *Mater. Sci. Eng.*, **1998**, *R22*, 1-55

4. Service, R.F; *Science*, **1996**, *273*, 878-880

5. Zhou, C.; Deshpande, M.R.; Reed, M.A.; Jones, II, L.; Tour, J.M.; *Appl. Phys. Lett.*, **1997**, *71*, 611-613

6. Reed, M.A.; *Proc. IEEE*, **1999**, *87*, 652-658

7. Chen, J.; Reed, M.A.; Rawlett, A.M.; Tour, J.M.; *Science*, **1999**, *286*, 1550-1552

8. Friend, R.; Burroghes, J.; Shimoda, T.; *Physics World*, **June 1999**, *12*, 35-40

9. Friend, R.H.; Gymer, G.W.; Holmes, A.B.; Burroughes, J.H.; Marks, R.J.; Taliani, C; Bradley, D.D.C.; Dos Santos, D.A.; Brédas, J.L.; Lögdlund, M.; Salaneck, W.R.; *Nature*, **1999**, *397*, 121-128

10. Bumm, L.A.; Arnold, J.J.; Dunbar, T.D.; Allara, D.L.; Weiss, P.S.; *J. Phys. Chem. B*, **1999**, *103*, 8122-8127

11. Tour, J.M.; *Acc. Chem. Res.*, **2000**, *33*, 791-804

12. Reed, M.A.; Chen, J.; Rawlett, A.M.; Price, D.W.; Tour, J.M.; *Appl. Phys. Lett.*, **2001**, *78*, 3735-3637

13. Xu, T; Peyerson, I.R.; Lakishikantham, M.V.; Metzger, R.M.; *Agnew. Chem. Int. Ed.*, **2001**, *40*, 1749-1752

14. Metzger, R.M.; Xu, T.; Peterson, I.R.; *J. Phys. Chem. B*, **2001**, *105*, 7280-7290

15. Liang, W.; Shores, M.P.; Bockrath, M.; Long, J.R.; Park, H.; *Nature*, **2002**, *417*, 725-

729

16. Babel, A.; Jenekhem S.A.; *J. Phys. Chem. B*, **2002**, *106*, 6129-6132

17. Allara, D.L.; Dunbar, T.D.; Weiss, P.S.; Bumm, L.A.; Cygan, M.T.; Tour, J.M.; Reinerth, W.A.; Yao, Kozaki, M.; Jones, II, L.; *Ann. NY Acad. Sci.*, **1998**, *852*, 349-370

18. Tarlov, M.J.; *Langmuir*, **1992**, *8*, 80-89

19. Jung, D.R.; Czanderna, A.W.; *Crit. Rev. Solid State*, **1994**, *19*, 1-54

20. Konstadinis, K.; Zhang, P.; Opila, R.L.; Allara, D.L.; *Surf. Sci.*, **1995**, *338*, 300-312

21. Jung, D.R.; Czanderna, A.W.; *Z. Phys. Chem.*, **1997**, *20*, 163-196

22. Jung, D.R.; Czanderna, A.W.; Herdt, G.C.; *J. Vac. Sci. Technol. A*, **1996**, *14*, 1779-1787

23. Herdt, G.C.; Czanderna, A.W.; *J. Vac. Sci. Technol. A*, **1997**, *15*, 513-519

24. Herdt, G.C.; Czanderna, A.W.; *J. Vac. Sci. Technol. A*, **1999**, *17*, 3415-3418

25. Dake, L.S.; King, D.E.; Czanderna, A.W.; *Solid State Sci.*, **2000**, *2*, 781-*789*

26. Hooper, A.; Fisher, G.L.; Konstadinidia, K.; Jung, D.; Nguyen, H.; Opila, R.; Collins, R.W.; Winograd, N.; Allara, D.L.; *J. Am. Chem. Soc.*, **1999**, *121*, 8052-8064

27. Fisher, G.L.; Hooper, A.E.; Opila, R.L.; Allara, D.L.; Winograd, N.; *J. Phys. Chem. B*, **2000**, *104*, 3267-3273

28. Fisher, G.L.; Walker, A.V.; Hooper, A.E.; Tighe, T.B.; Bahnck, K.B.; Skriba, H.T.; Reinard, M.D.; Haynie, B.C.; Opila, R.L.; Winograd, N.; Allara, D.L.; *J. Am. Chem. Soc.*, **2002**, *124*, 5528-5541

29. Lisy, J.M.; *Int. Rev. Phys. Chem.*, **1997**, *16*, 267-289

30. Niedner-Schatteburg, G.; Bondybey, V.E.; *Chem. Rev.*, **2000**, *100*, 4059-4086

31. Duncan, M.A.; *Int. J. Mass Spectrom.*, **2000**, *200*, 545-569

32. *Advanced Inorganic Chemistry: Sixth Edition*; Cotton, F.A.; Wilkinson, G; Murillo, C.A.; Bochmann, M.; John Wiley and Sons , Inc.: **1999**

33.Tachibana, T.; Williams, B.E.; Glass, J.T.; *Phys. Rev. B*, **1992**, *45*, 11968-11974

34. Angelpoulos, M; *IBM J. Res. & Dev.*, **2001**, *45*, 57-75

35. Monteiro, O.R.; *J. Vac. Sci. Technol. B*, **1999**, *17*, 1094-1097

36. Walker, A.V.; Tighe, T.B.; Reinard, M.D.; Haynie, B.C.; Allara, D.L.; Winograd, N.; *Chem. Phys. Letts.*, **2003**, *369*, 615-620

37. Nuzzo, R.G.; Allara, D.L.; *J. Am. Chem. Soc.*, **1983**, *105*, 4481-4483

38. Bain, C.D.; *Self-Assembled Monolayer Films of Thiols on Gold*, Ph. D. Thesis, Harvard University, **1989**

39. Nuzzo, R.G.; Dubois, L.H.; Allara, D.L.; *J. Am. Chem. Soc.*, **1990**, *112*, 558-569

40. Laibinis, P.E.; Whitesides, G.M.; Allara, D.L.; Tao, Y.T.; Parikh, A.N.; Nuzzo, R.G.; *J. Am. Chem. Soc.*, **1991,** *113*, 7152-7167

41. Xu, C.J.; Sun, L.; Kepley, L.J.; Crooks, R.M.; Ricco, A.J.; *Anal. Chem.*, **1993**, *65*, 2102-2107

42. Laibinis, P.E.; Bain, C.D.; Nuzzo, R.G.; Whitesides, G.M.; *J. Phys. Chem.*, **1995,** *99*, 7663-7676

43. Tour, J.M.; Jones II, L.; Pearson, D.L.; Lamba, J.J.S.; Burgin, T.P.; Whitesides, G.M.; Allara, D.L.; Parikh, A.N.; Atre, S.V.; *J. Am. Chem. Soc.*, **1995**, *117*, 9529-9534

44. Fryxell, G.E.; Rieke, P.C.; Halverson, A.; *Langmuir*, **1996**, *12*, 5064-5075

45. Leff, D.V.; Brandt, L.; Heath, J.R.; *Langmuir*, **1996**, *12*, 4723-4730

46. Braun, R.M.; Blenkinsopp, P.; Mullock, S.J.; Corlett, C.; Willey, K.F.; Vickerman, J.C.; Winograd, N.; *Rapid Commun. Mass. Spec.*, **1998**, *12*, 1246-1252

47. Beamson, G.; Briggs, D.; Davies, S. F.; Fletcher, I. W.; Cark, D. T.; Howard, J.; Gelius, U.; Wannberg, B.; Balzer, P. *Surf. Int. Anal.* **1990**, *15*, 541-549.

48. Gelius, U.; Wannberg, B.; Baltzer, P.; Fellnerfeldegg H.; Carlsson, G.; Johansson, C. G.; Larsson, J.; Munger, P.; Vegerfors, G. *J. Elec. Spec. Rel. Phenom.* **1990**, *52*, 747-785

49. Gaussian 98, Revision A.9, Frisch, M.J.; Trucks, G.W.; Schlegel, H.B.; Scuseria, G.E.;Robb, M.A.;Cheeseman, J.R.; Zakrzewski, V.G.; Montgomery Jr, J.A.; Stratmann, R.E.; Burant, J.C.; Dapprich, S.; Millam, J.M.; Daniels, A.D.; Kudin, K.N.O.; Strain, F.M.C.; Farkas, O.; Tomasi, J.; Barone, V.; Cossi, M.; Cammi, R.; Mennucci, B.; Pomelli, C.; Adamo, C.; Clifford, S.; Ochterski, J.; Petersson, G.A.; Ayala, P.Y.; Cui, Q.; Morokuma, K.; Malick, D.K.; Rabuck, A.D.; Raghavachari, K.; Foresman, J.B.; Cioslowski, J.; Ortiz, J.V.; Baboul, A.G.; Stefanov, B.B.; Liu, G.; Liashenko, A.; Piskorz, P.; Komaromi, I.; Gomperts, R.; Martin, R.L.; Fox, D.J.; Keith, T.; Al-Laham, M.A.; Peng, C.Y.; Nanayakkara, A.; Challacombe, M.; Gill, P.M.W.; Johnson, B.; Chen, W.; Wong, M.W.; Andres, J.L.; Gonzalez, C.; Head-Gordon, M.; Replogle, E.S.; Pople, J.A.; Gaussian Inc., Pittsburgh PA, 1998

50. Legge, F. S.; Nyberg, G. L.; Peel, J. B.; *J. Phys. Chem. A*, **2001**, *105*, 7905-7916

51.(a) Seminario, J. M.; Zacarias, A. G.; Tour, J. M.; *J. Phys. Chem. A*, **1999**, *103*, 7883-7887; (b) Seminario, J. M.; Zacarias, A. G.; Tour, J. M.; *J. Am. Chem. Soc.*, **1999**, *121*, 411-416

52. Fängström, T.; Lunell, S.; Kasai, P. H.; Eriksson, L. A.; *J. Phys. Chem. A*, **1998**, *102*, 1005-1007

53. Sakai, S.; *J. Phys. Chem.*, **1992**, *96*, 8369-8373

54. Sakai, S.; *J. Phys. Chem.*, **1993**, *97*, 8917-8921

55 . Parnis, J. M.; Mitchell, S. A.; Rayner, D. M.; Hackett, P. A.; *J. Phys. Chem.*, **1988**, *92*, 3869-3874.

56. Dubois, L.H.; Nuzzo, R.G.; *Ann. Rev. Phys. Chem.*, **1992**, *43*, 437-463

57 . Tarlov, M.J.; Neuman, J.G.; *Langmuir*, **1992**, *8*, 1398-1405

58. Hagenhoff, B.; Benninghoven, A.; Spinke, J.; Liley, M.; Knoll, W.; *Langmuir*, **1993**, *9*, 1622-1624

59. Wood, M.C.; Surface Characterization and Imaging with Ion-Induced Desorption and Multiphoton Resonance Ionization, Ph.D. Thesis, The Pennsylvania State University, **1995**

60. Hooper, D.A.; Cooper, E.; Leggett, G.J.; *J. Phys. Chem. B.*, **1998**, *102*, 174-184

61. Ohgi, T.; Sheng, H.-Y.; Dong, Z.-C.; Nejoh, H.; *Surf. Sci.*, **1999**, *442*, 277-282

62. Konstadinidis, K.; Zhang, P.; Opila, R.L; Allara, D.L.; *Surf. Sci.*, **1995**, *338*, 300-312

63. In contrast, we have observed that for other deposited metal atoms, e.g. Mg, do desorb with a high probability from the $-OCH_3$ SAM surface under similar deposition conditions to the present experiments.

A.V. Walker, T.B. Tighe O. Cabarcos, B.C. Haynie, D.L. Allara, N. Winograd, in preparation

64. We have evidence that the orientation of the $-OCH_3$ group does change the apparent reactivity of deposited metal atoms. An indication of the orientation of the methoxy group relative to the methylene backbone is given by the ratio of the intensity of the d^- CH_2 stretch (2918 cm^{-1}) to the C-O stretch (1132 cm^{-1}). Upon Al deposition for a SAM layer with a ratio of 1:2 (d^- CH_2 str.:C-O str.) larger changes in the IR spectra are observed than for a layer with a 1:1 ratio indicating that the deposited Al has apparently different reactivities depending upon the orientation of the methoxy group.

65. The formation of transient defects and the subsequent diffusion of species is a common mechanism; such processes are operative for the diffusion of gases and other species through polymers ("Diffusion in Polymers"; Crank, J.; Park, G.S., eds.; Academic Press, 1968) and along interfaces ("Interfaces in Crystalline Materials"; Sutton, A.P.; Balluffi, R.W.; Clarendon Press, Oxford, 1995).

66. Shen, W.; Nyberg, G.L.; *Surf. Sci.*, **1993**, *296*, 49-56

67. Stranick, S.J.; Parikh, A.N.; Tao, Y.-T.; Allara, D.L.; Weiss, P.S.; *J. Phys. Chem.*, **1994**, *98*, 7636-7646

68. Terán Arce, F.; Vela, M.E.; Salvarezza, R.C.; Ariva, A.J.; *Electrochim. Acta*, **1998**, *44*, 1053-1067

69. The reaction energy is given by –

$$\begin{aligned}\Delta E &= \text{E(bonds made)} - \text{E(bonds broken)} \\ &= \text{E}(\text{Au}-\text{S}(\text{CH}_2)_5\text{OCH}_3) + \text{E}(\text{Al}-\text{Au}-\text{S}(\text{CH}_2)_5\text{OCH}_3) \\ &\quad - \text{E}(\text{Al}-\text{S}(\text{CH}_2)_5\text{OCH}_3) - \text{E}(\text{Al}-\text{Au}-\text{S}(\text{CH}_2)_5\text{OCH}_3) \\ &= -(179 + 200 - 293 - 164)\ \text{kJ mol}^{-1} \\ &= +78\ \text{kJ mol}^{-1}\end{aligned}$$